Figure1-13.

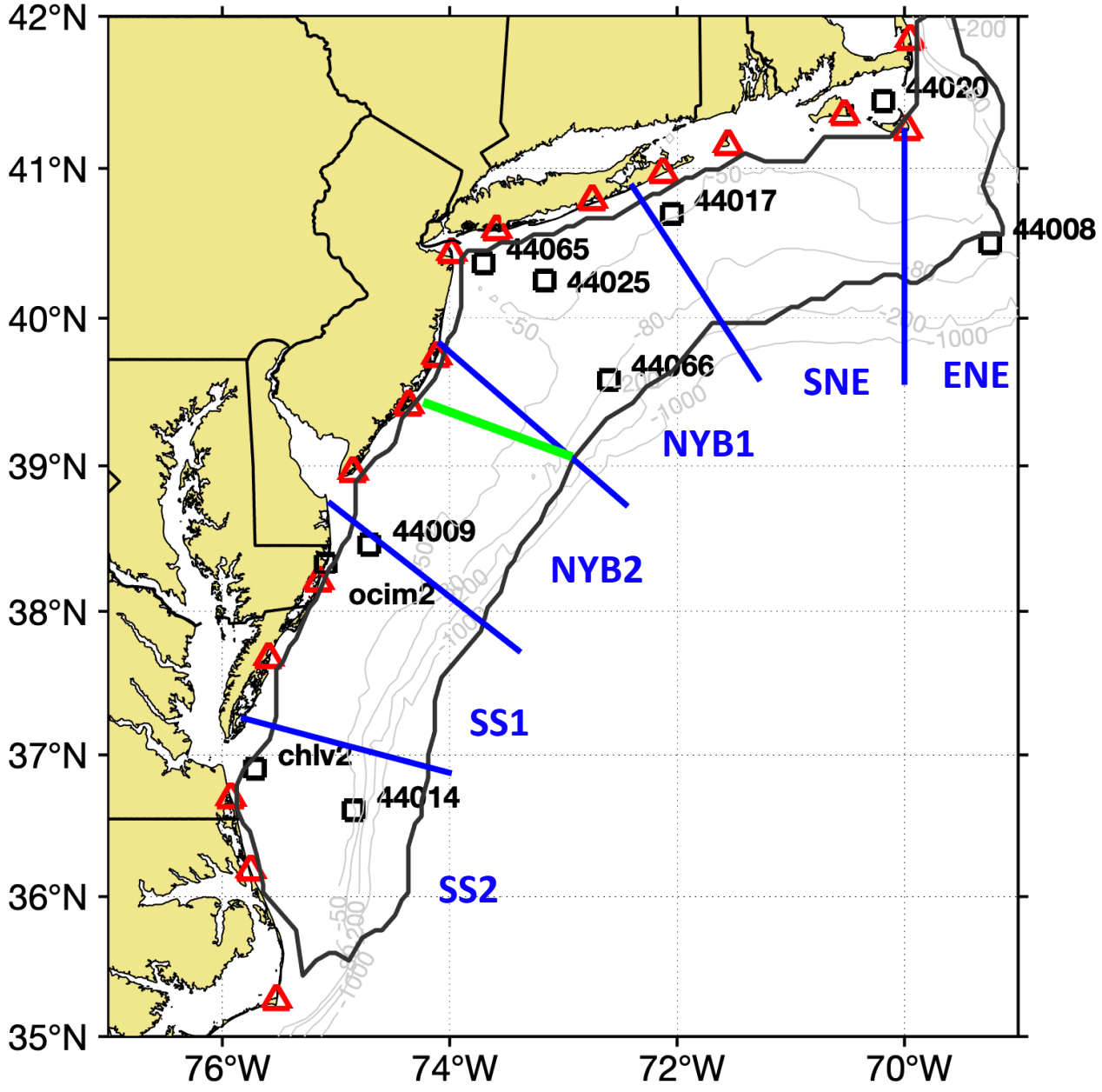
42°N
41°N
40°N
39°N
38°N
37°N
36°N
35°N
76°W
74°W
72°W
70°W
44020
44017
44008
44065
44025
44066
44009
ocim2
chlv2
44014
SNE
ENE
NYB1
NYB2
SS1
SS2

Figure 1

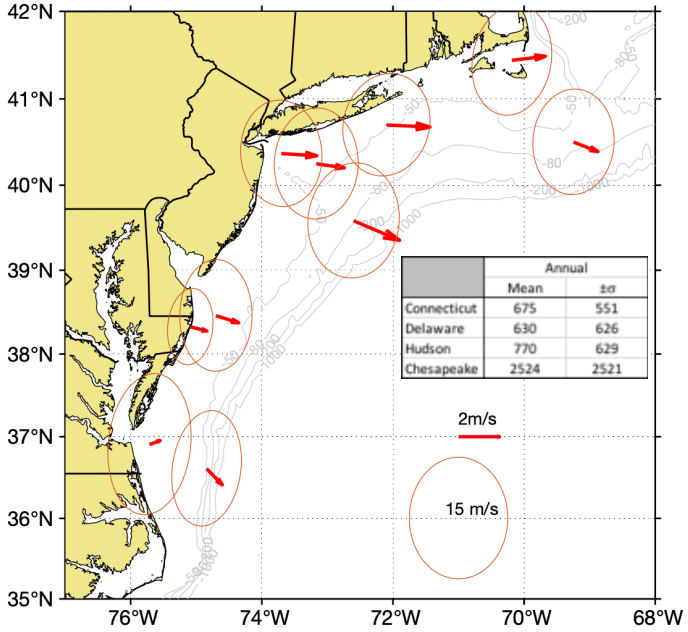

a)

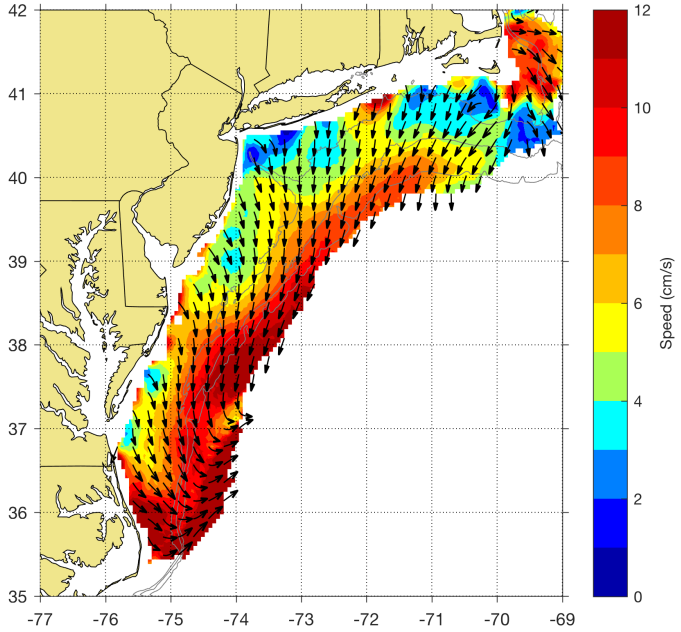

b)

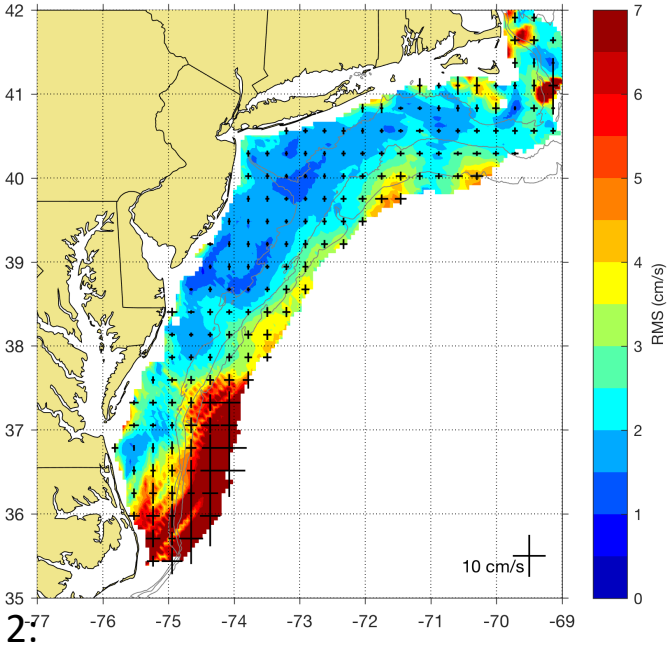

c)

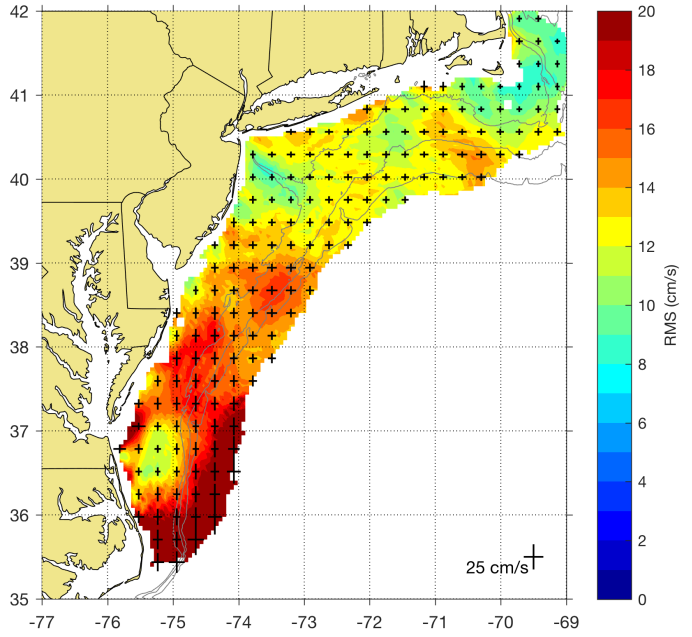

d)

Figure 2.

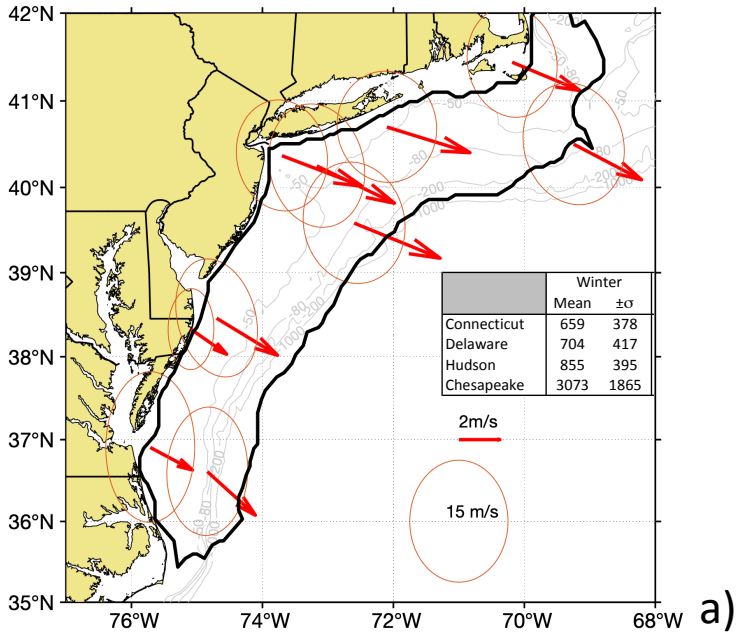

a)

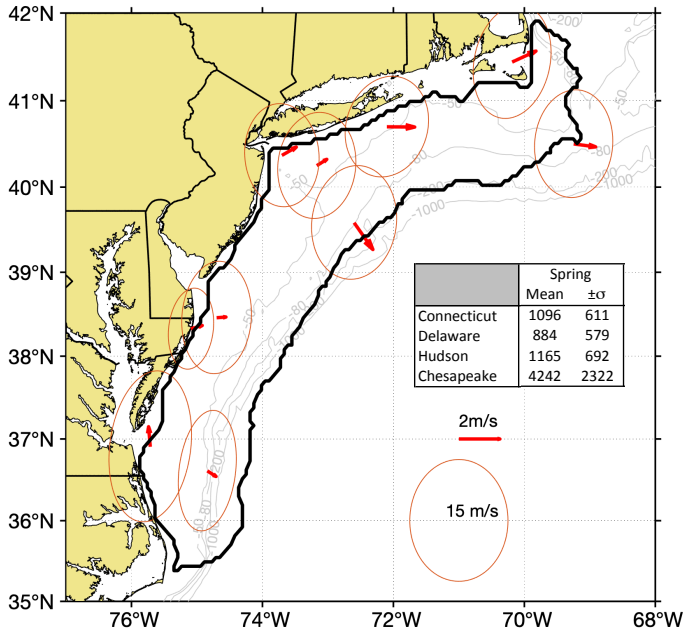

b)

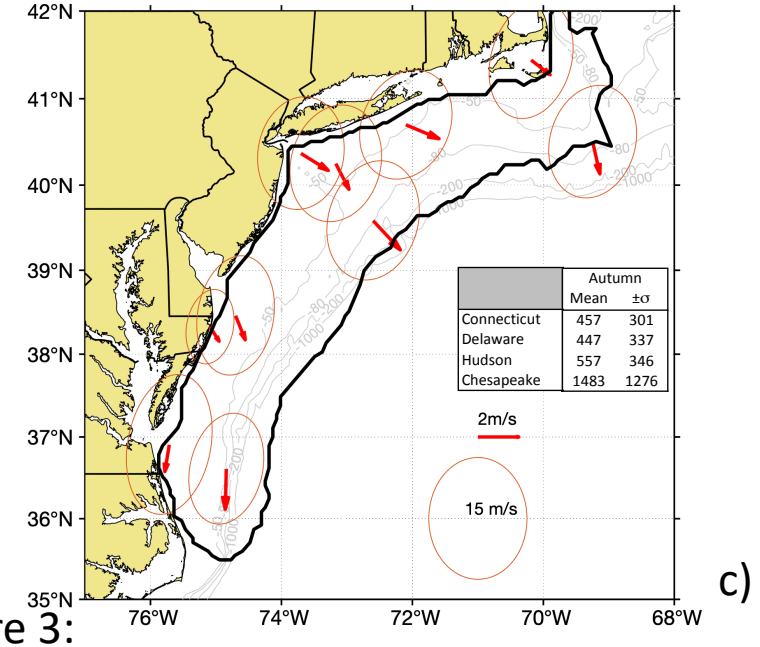

c)

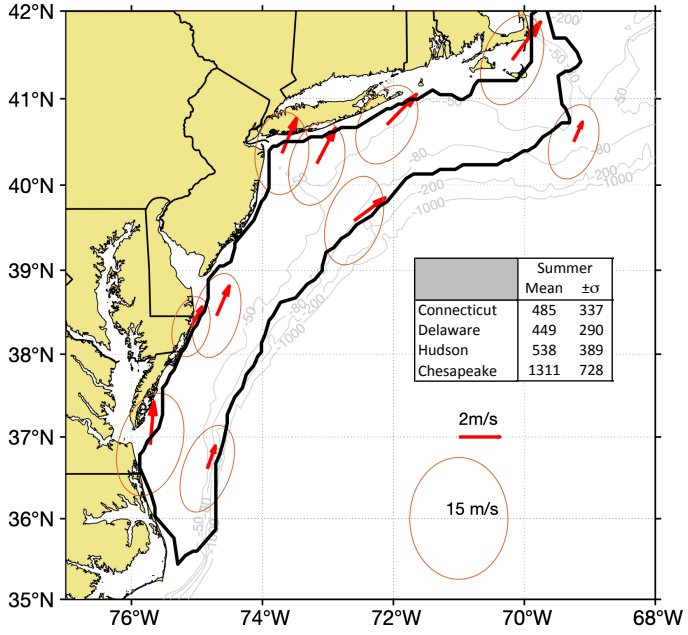

d)

Figure 3:

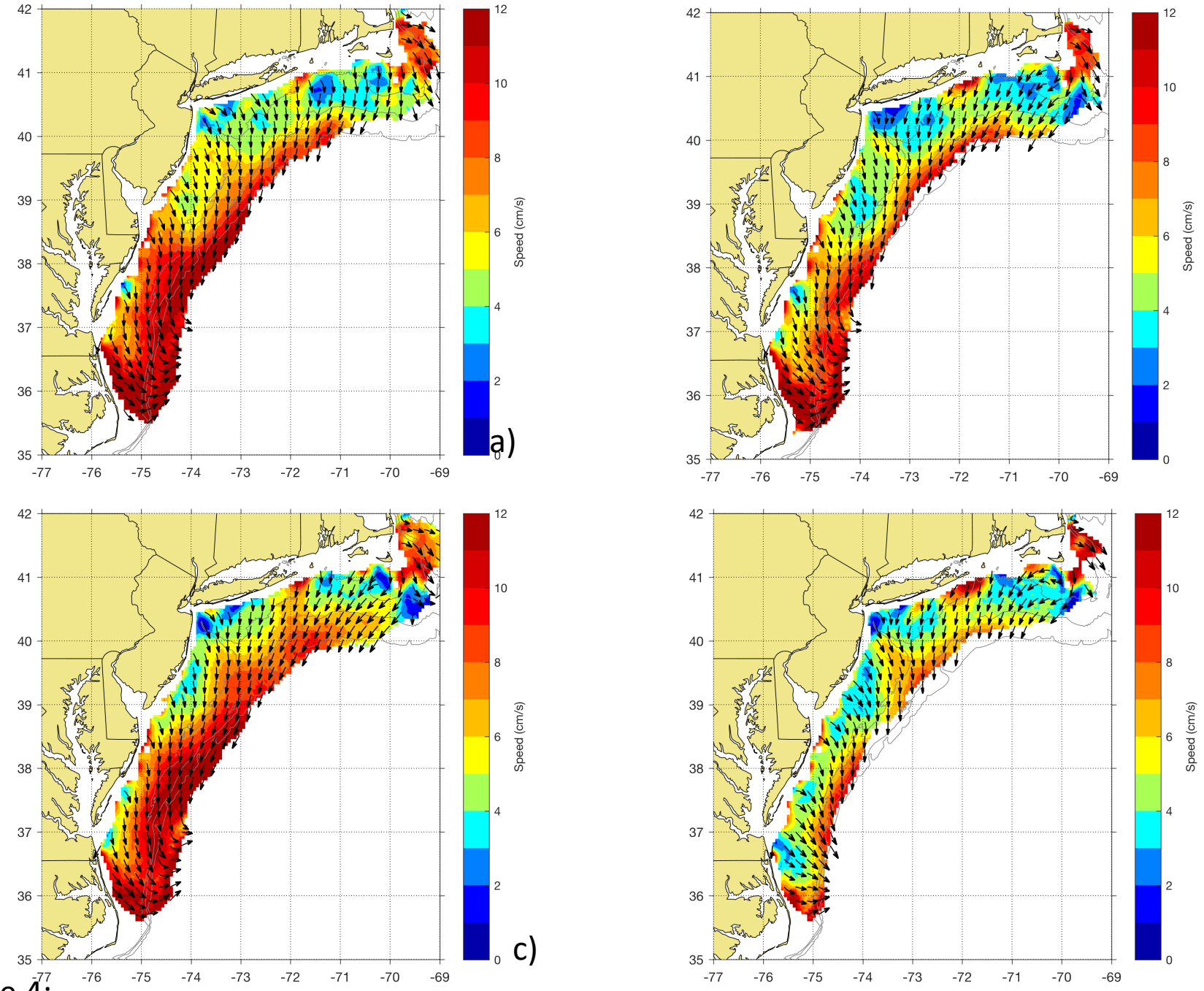
a)
b)
c)
d)
Speed (cm/s)
0
2
4
6
8
10
12
35
36
37
38
39
40
41
42
-77
-76
-75
-74
-73
-72
-71
-70
-69

Figure 4:

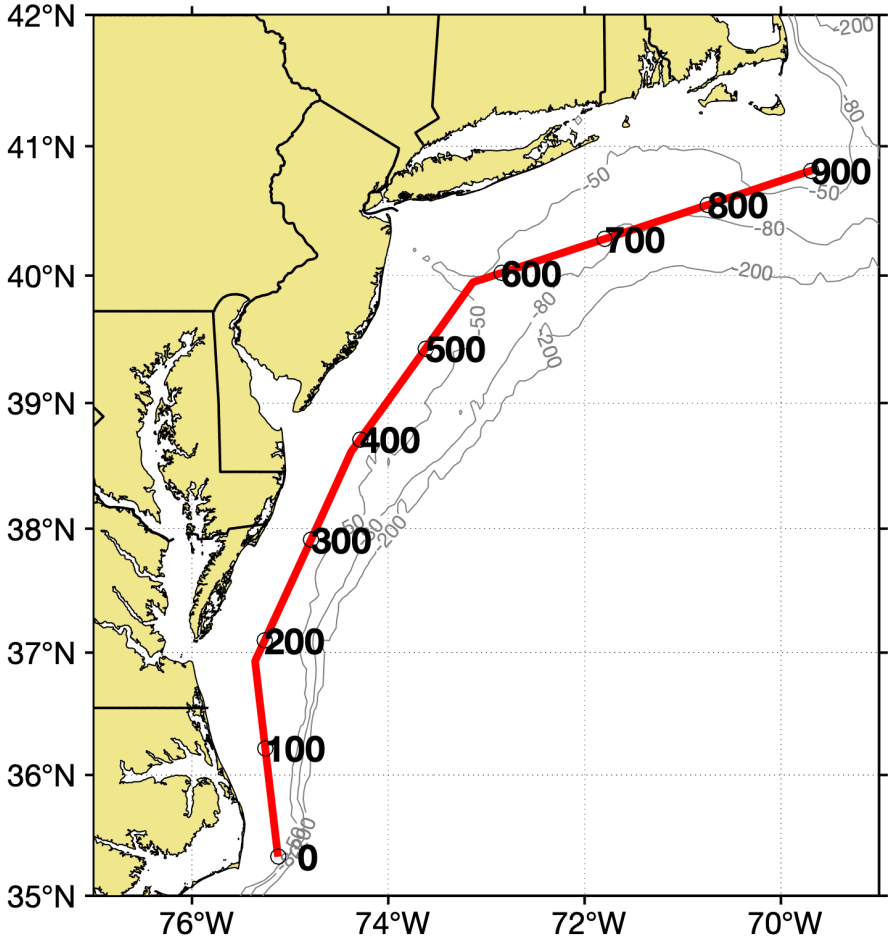
42°N
41°N
40°N
39°N
38°N
37°N
36°N
35°N
76°W
74°W
72°W
70°W
0
100
200
300
400
500
600
700
800
900
-200
-80
-50

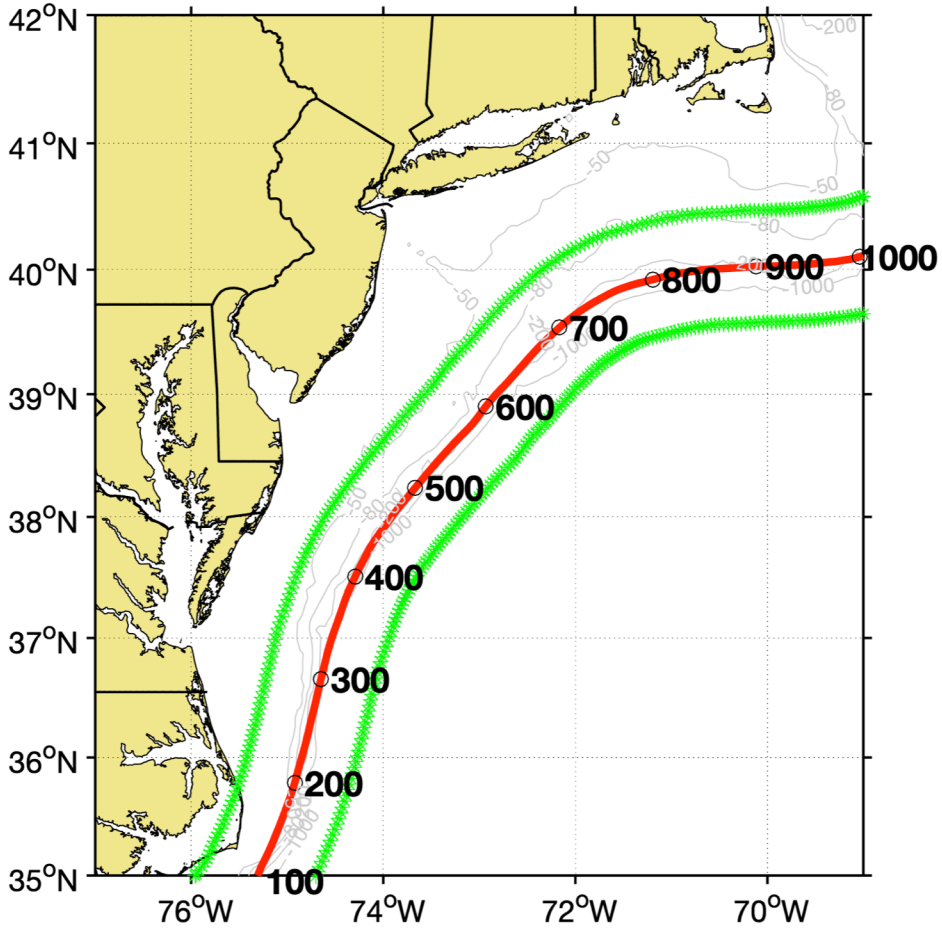
42°N
41°N
40°N
39°N
38°N
37°N
36°N
35°N
76°W
74°W
72°W
70°W
100
200
300
400
500
600
700
800
900
1000
-200
-80
-50

b)

Figure 5:

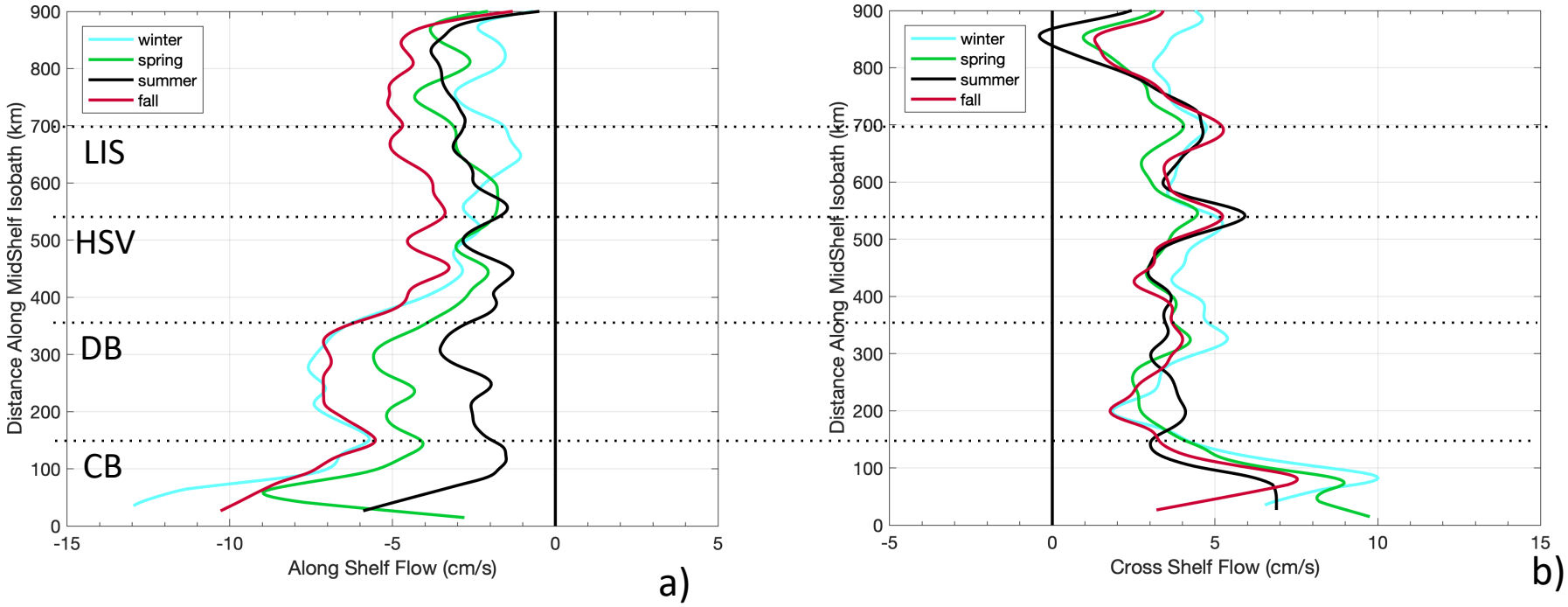
winter
spring
summer
fall
LIS
HSV
DB
CB
Distance Along MidShelf Isobath (km)
Along Shelf Flow (cm/s)
a)
Cross Shelf Flow (cm/s)
b)

Figure 6:

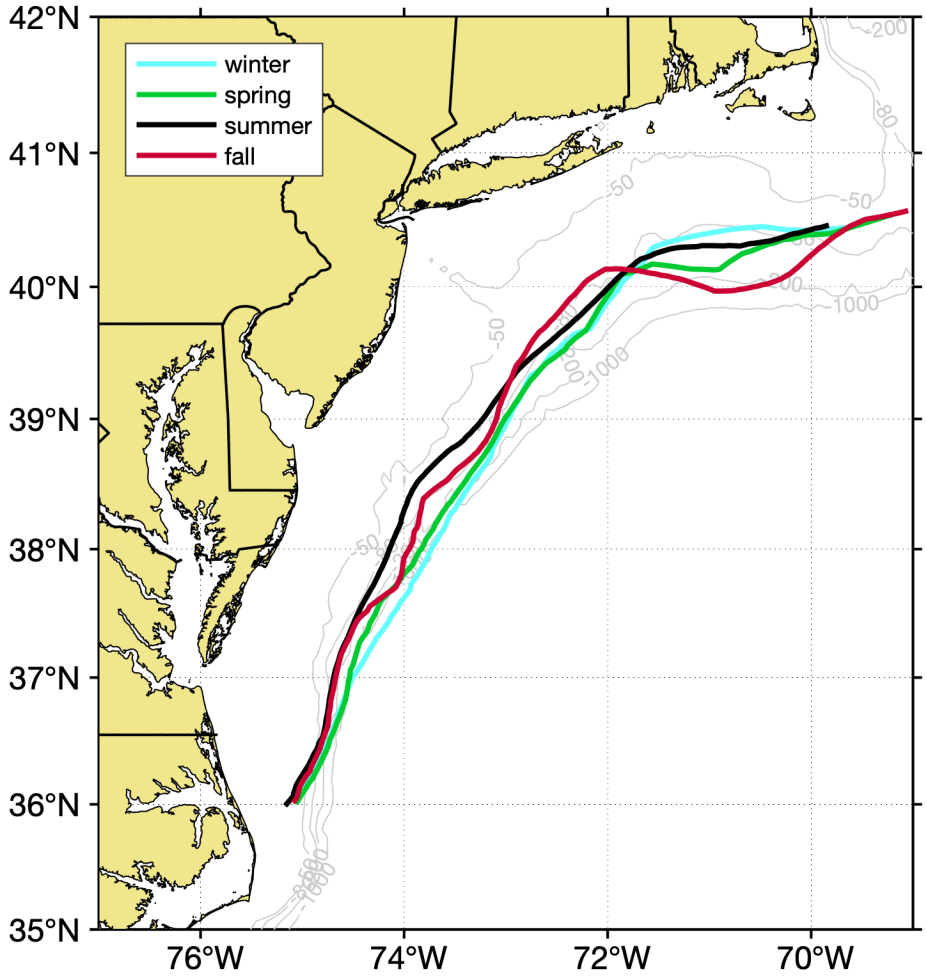

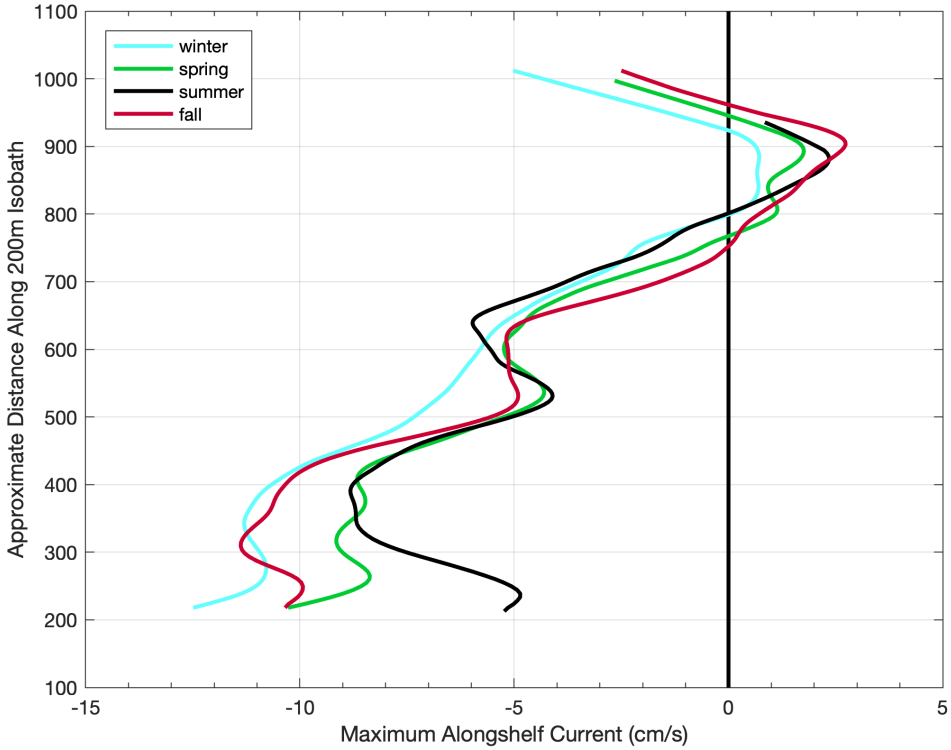

b)

Figure 7: Maximum alongshelf current a) location and b) magnitude

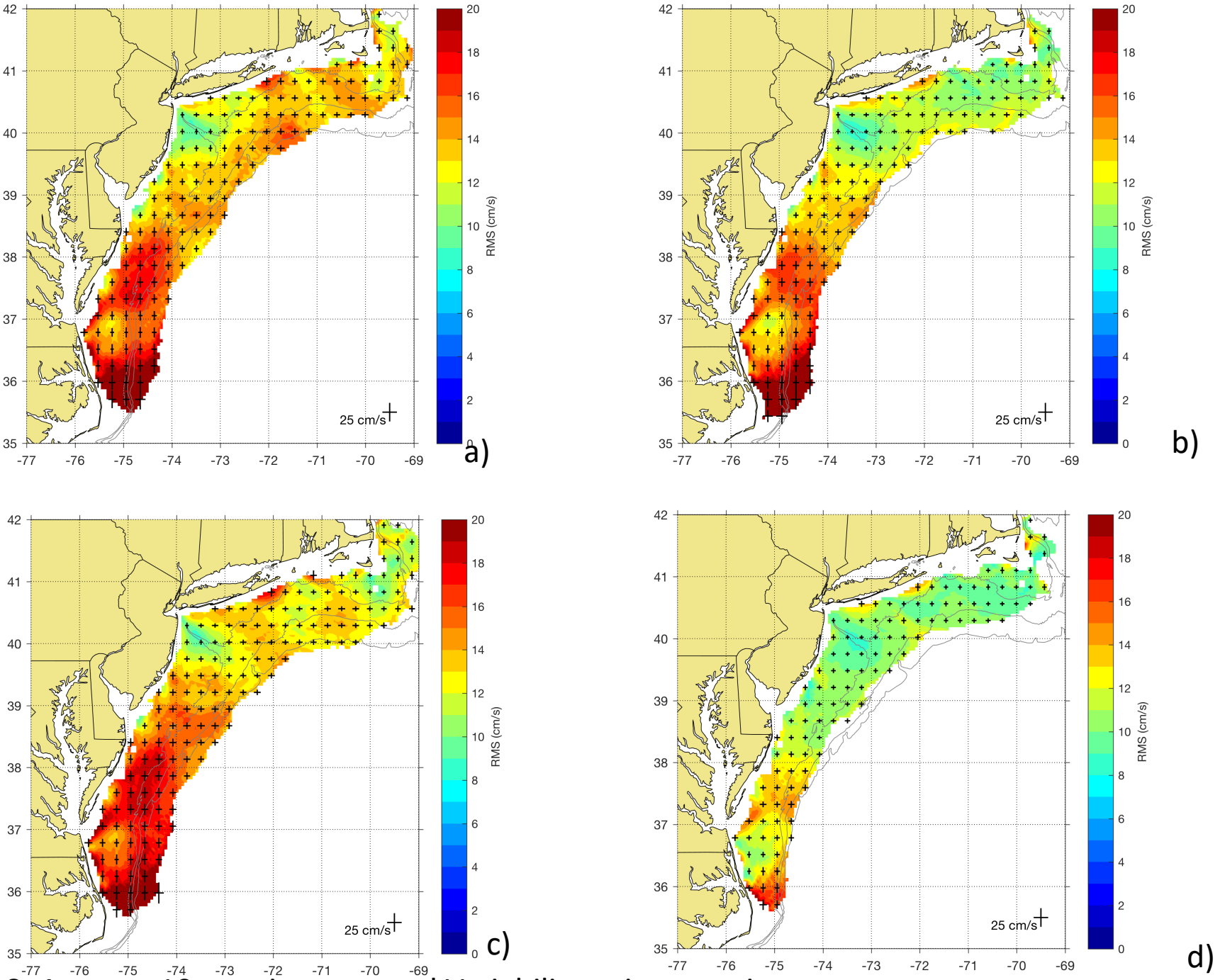

Figure 8: Average 10 year intra-annual Variability: winter, spring, summer, autumn

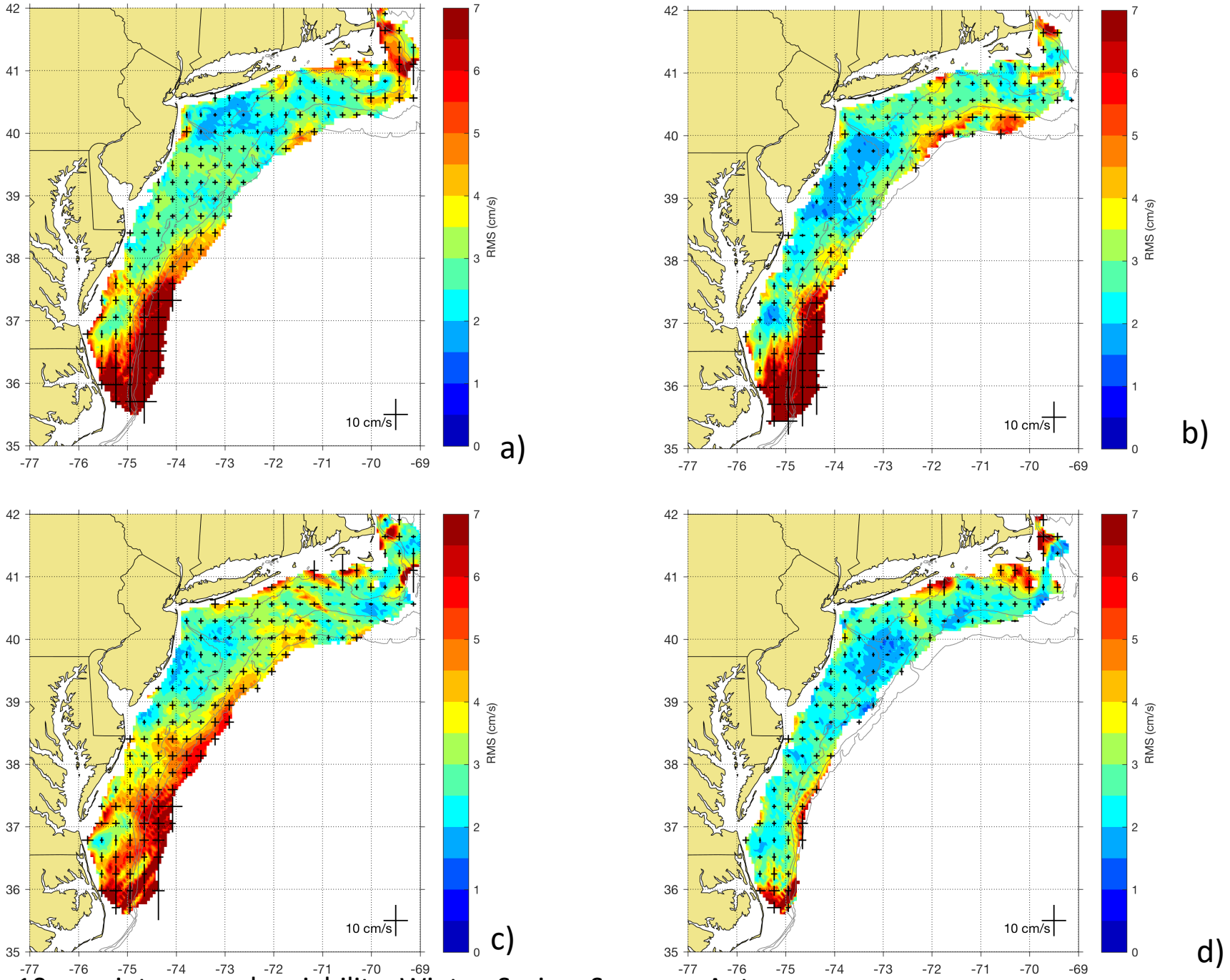

Figure 9: 10 year interannual variability: Winter, Spring, Summer, Autumn

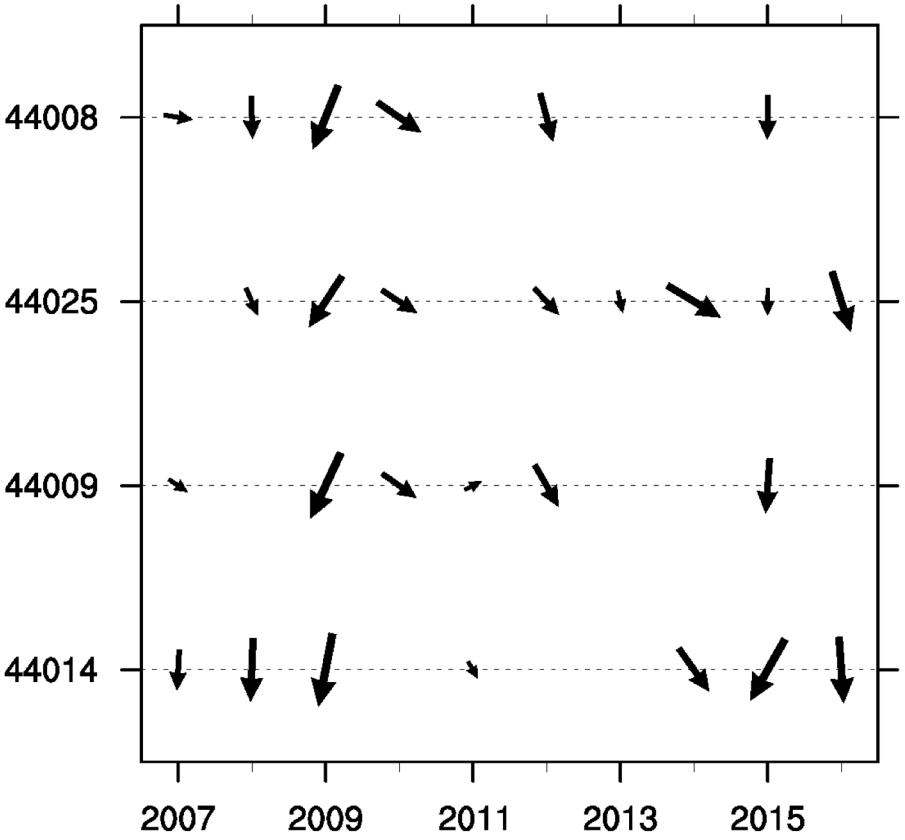
44008
44025
44009
44014
2007
2009
2011
2013
2015

a)

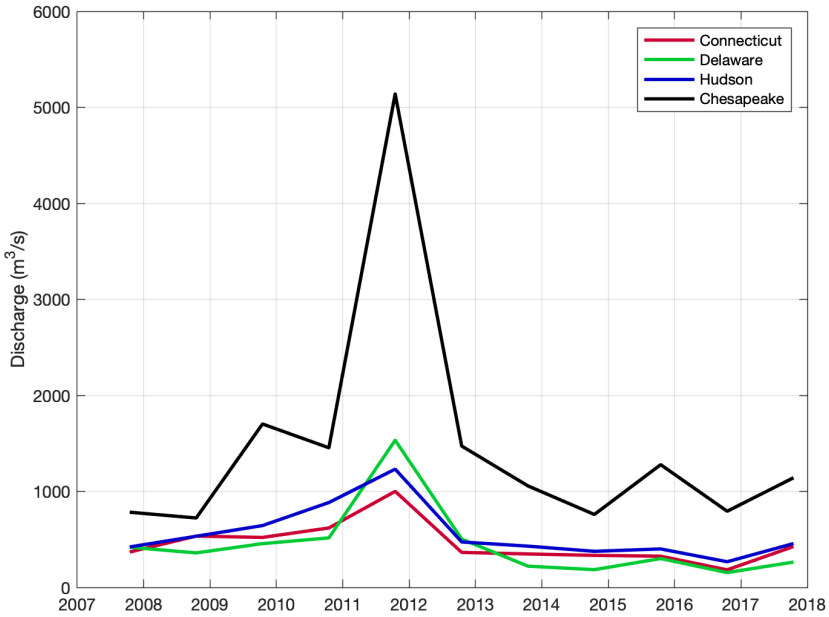
Connecticut
Delaware
Hudson
Chesapeake
Discharge (m3/s)
6000
5000
4000
3000
2000
1000
0
2007
2008
2009
2010
2011
2012
2013
2014
2015
2016
2017
2018

b)

Figure 10:

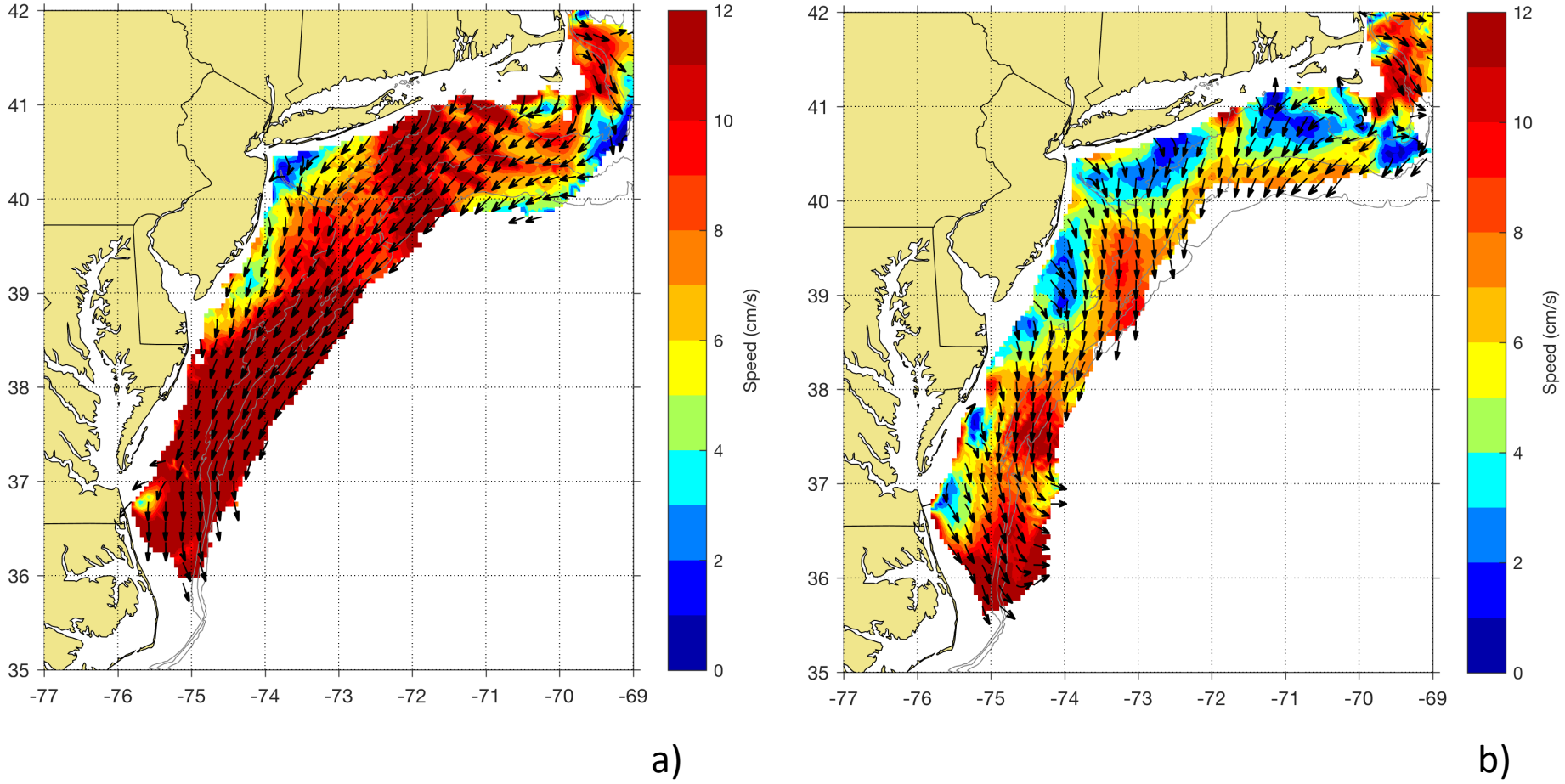
42
41
40
39
38
37
36
35
-77
-76
-75
-74
-73
-72
-71
-70
-69
12
10
8
6
4
2
0
Speed (cm/s)
a)
b)

Figure 11:

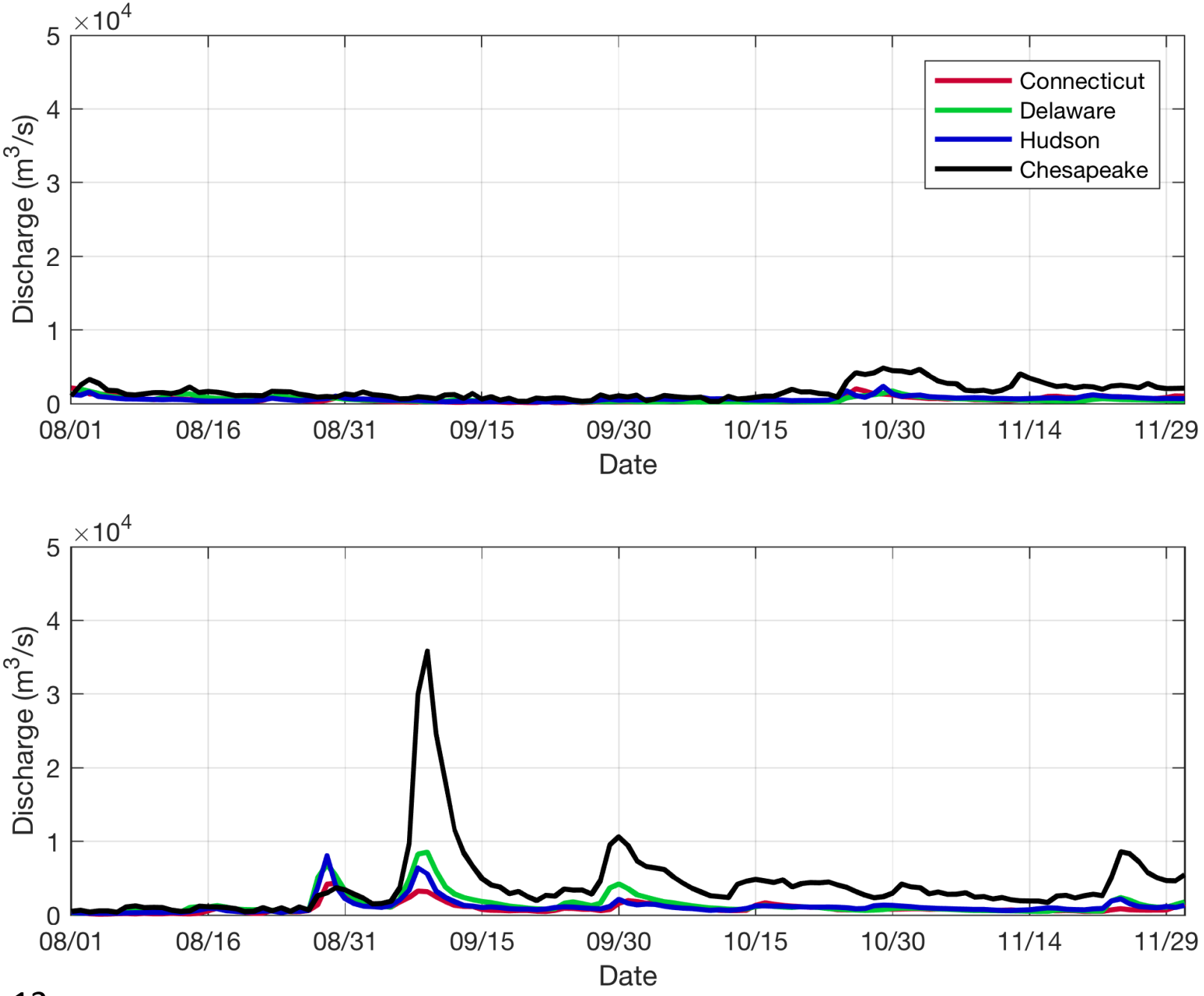
×10^4
5
4
3
2
1
0
Discharge (m^3/s)
Connecticut
Delaware
Hudson
Chesapeake
08/01
08/16
08/31
09/15
09/30
10/15
10/30
11/14
11/29
Date
×10^4
5
4
3
2
1
0
Discharge (m^3/s)
08/01
08/16
08/31
09/15
09/30
10/15
10/30
11/14
11/29
Date

Figure 12:

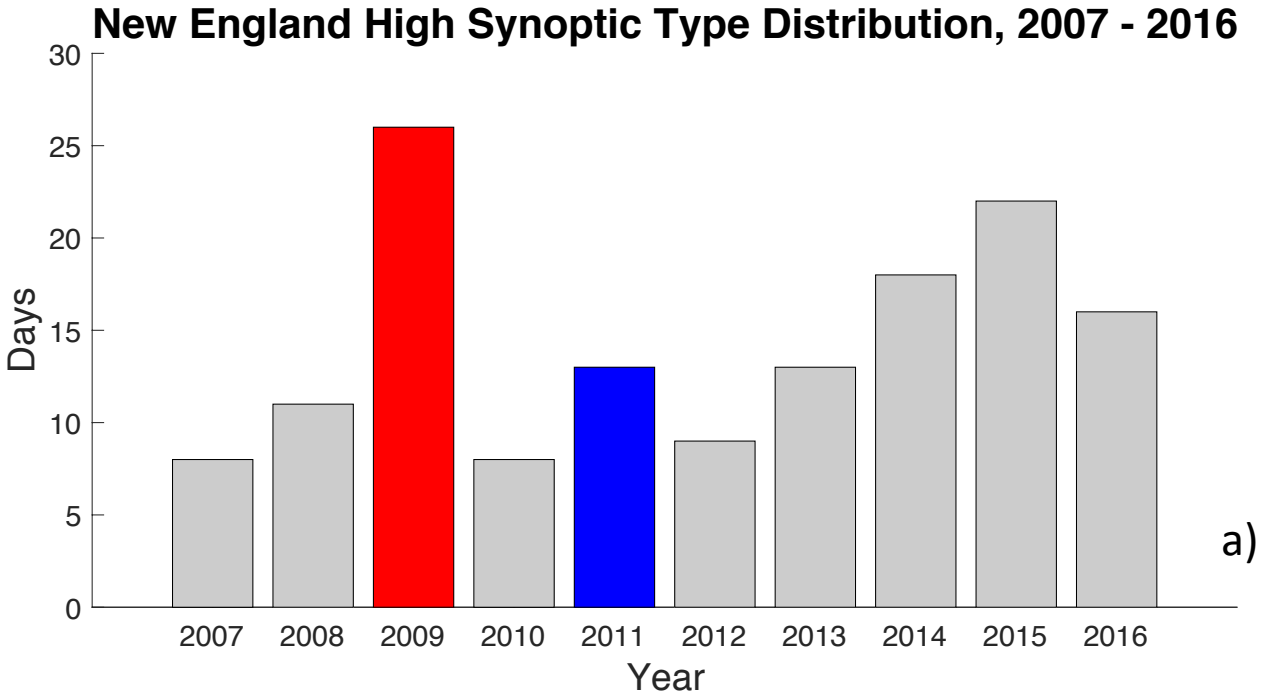
New England High Synoptic Type Distribution, 2007 - 2016
Days
Year
0
5
10
15
20
25
30
2007
2008
2009
2010
2011
2012
2013
2014
2015
2016
a)

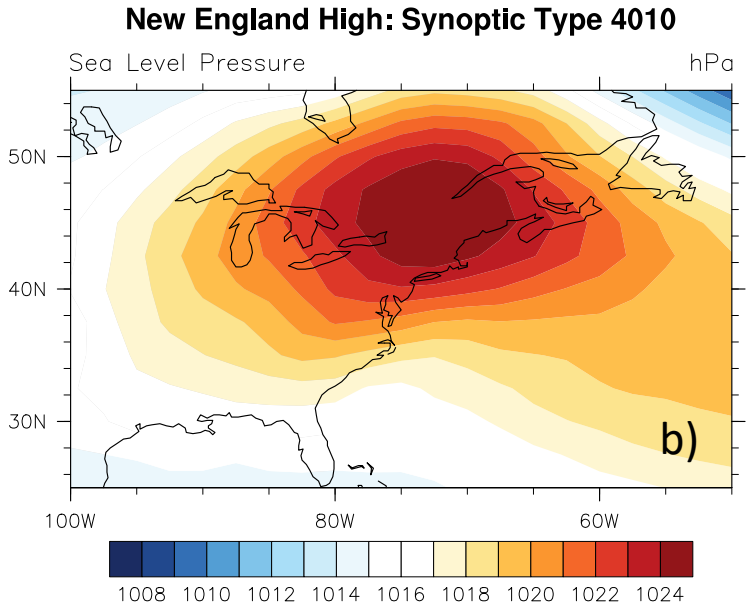
New England High: Synoptic Type 4010
Sea Level Pressure
hPa
50N
40N
30N
100W
80W
60W
b)
1008
1010
1012
1014
1016
1018
1020
1022
1024

Figure 13:

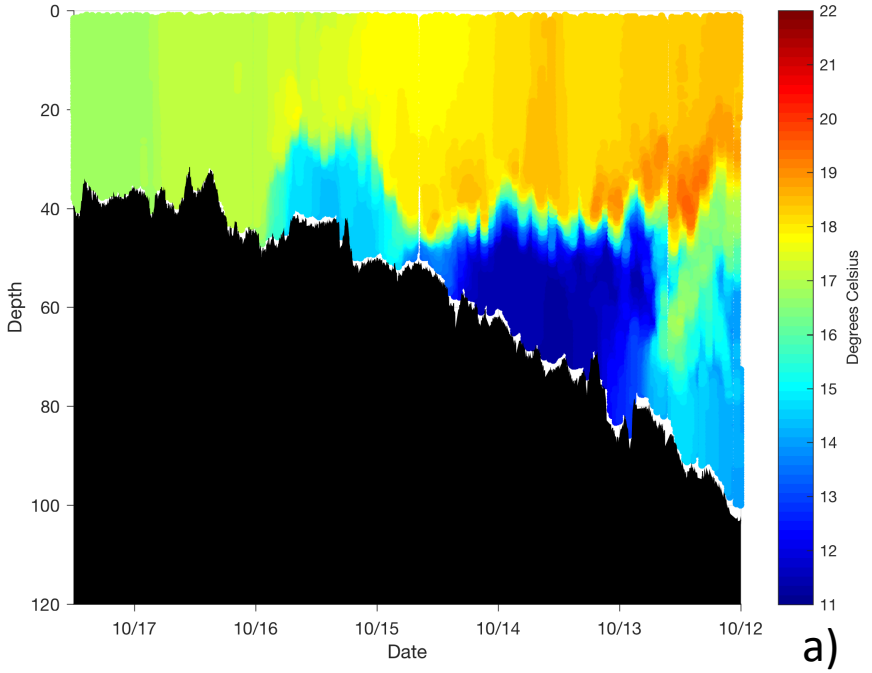

a)

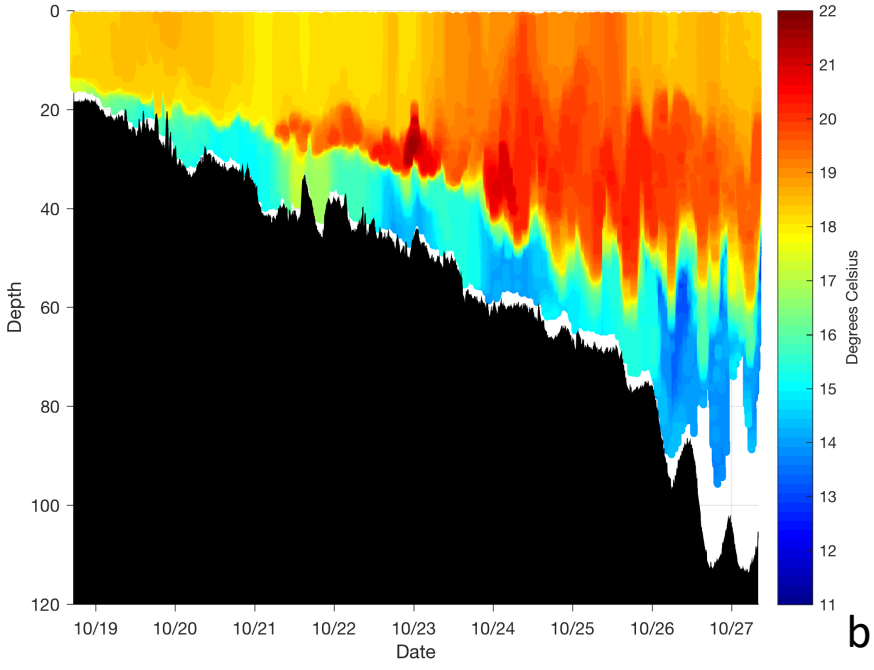

b)

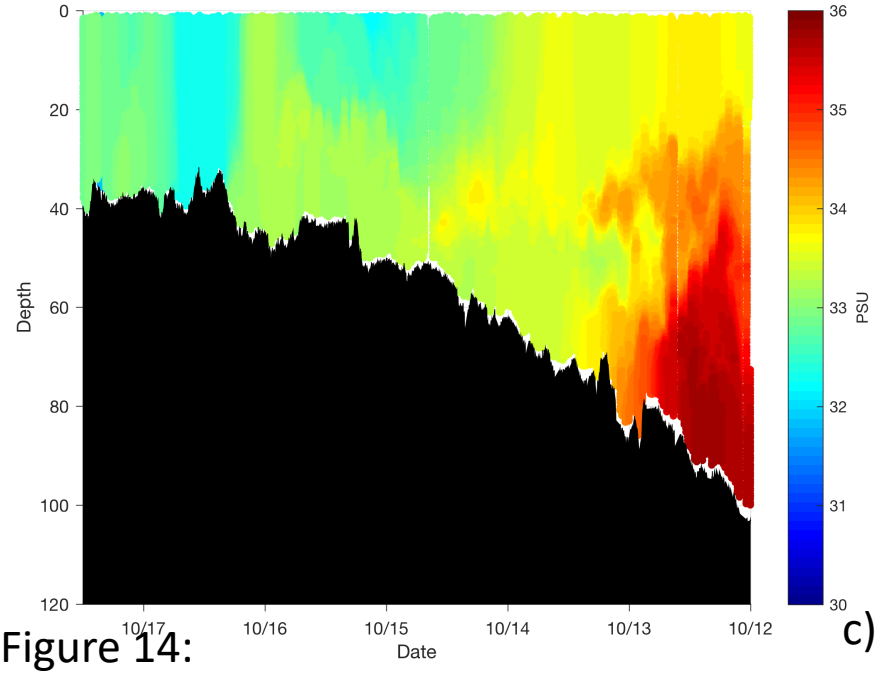

c)

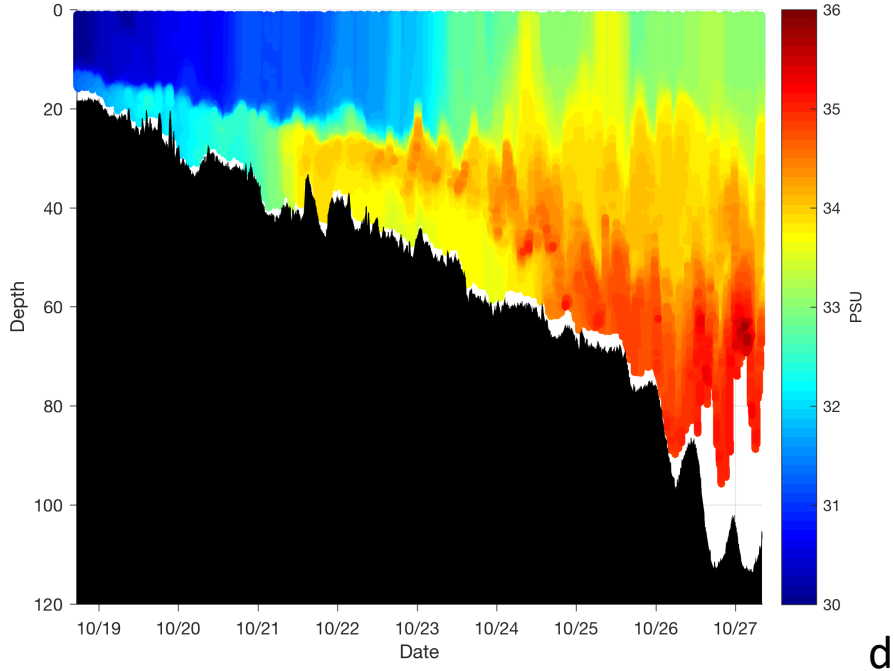

d)

Figure 14:

MAB Current Figures

As of May 1, 2020

Fig 1-9 results, Fig 10-14 discussion

Annual and Seasonal Surface Circulation over the Mid Atlantic Bight Continental Shelf Derived from a Decade of High Frequency Radar Observations

Hugh Roarty, Scott Glenn, Joseph Brodie, Laura Nazzaro, Michael Smith, Ethan Handel, Josh Kohut

Center for Ocean Observing Leadership, Rutgers University, New Brunswick, NJ, USA.

Teresa Updyke, Larry Atkinson

Center for Coastal Physical Oceanography, Old Dominion University, Norfolk, VA, USA.

William Boicourt

Center for Environmental Science, University of Maryland, Cambridge

Wendell Brown

School for Marine Science and Technology, University of Massachusetts Dartmouth, New Bedford, MA, USA.

Harvey Seim, Mike Muglia

University of North Carolina**,** East Carolina University Department of Coastal Studies

Haixing Wang, Donglai Gong

Virginia Institute of Marine Science, College of William & Mary, Gloucester Point, VA, USA.

Author Contributions:

Conceptualization, HR, SG, JK; Data Curation MS, LN; Formal Analysis HR, JB, LN, MS, SG, JK, TU, WBr, HW, DG, EH; Funding Acquisition SG, WBr, WBo, LA, HS; Resources WBr, HS, MM, TU, LA, HR; Supervision HR, WBo; Visualization HR, JB, LN; Writing-original draft HR, SG, JK, HS, DG, TU, LA, JB

Draft May 2, 2020

Three Key Points

1) A decade of hourly surface current maps were used to calculate annual and seasonal means and interannual and intra-annual variability
2) Mean flows are crossshore near the coast and southward alongshore with greater speeds offshore
3) Wind velocity and river discharge are used to explain the most significant interannual variability

Abstract

A decade (2007-2016) of hourly 6 km resolution maps of the surface currents across the Mid Atlantic Bight (MAB) generated by a regional-scale High Frequency Radar network are used to reveal new insights into the spatial patterns of the annual and seasonal mean surface flows. Across the 10-year time series, temporal means, inter- and intra-annual variability are used to quantify the variability of spatial surface current patterns. The 10-year annual mean surface flows are weaker and mostly cross shelf near the coast, increasing in speed and rotating to more alongshore directions near the shelf break, and increasing in speed and rotating to flow off-shelf in the southern MAB. The annual mean surface current pattern is relatively stable year to year compared to the hourly variations within a year. The ten-year seasonal means exhibit similar current patterns, with winter and summer more cross-shore while spring and fall transitions are more alongshore. Fall and winter mean speeds are larger and correspond to when mean winds are stronger and cross-shore.

70 Summer mean currents are weakest and correspond to a time when the mean wind opposes
71 the alongshore flow. Again, intra-annual variability is much greater than interannual, with
72 the fall season exhibiting the most interannual variability in the surface current patterns.
73 The extreme fall seasons of 2009 and 2011 are related to extremes in the wind and river
74 discharge events caused by different persistent synoptic meteorological conditions,
75 resulting in more or less rapid fall transitions from stratified summer to well-mixed winter
76 conditions.

77

Plain Language Summary

A coordinated High Frequency Radar network operated between Cape Cod, MA and Cape Hatteras, NC generates hourly maps of ocean surface currents. A decade-long study revealed the detailed structure of the surface flows. These flows were compared to wind and river flow data to explain the patterns observed in the flow.

Near the coast the average currents flow offshore. Away from the coast the average currents flow along the coast towards the south. Fall is the season with the most variability from year to year. Its higher variability can be traced to different regional weather patterns that change the wind fields and the amount of freshwater delivered by the rivers to the coastal ocean.

This is the first study to use a decade of observed surface current maps that uniquely and simultaneously observe the changing patterns of the average flow structure along a segment of eastern United States. The improved understanding of the coastal circulation over a wide area, and what drives its variability, has implications for pollutant transport, plankton transport at the base of the food chain, fish and shellfish reproduction, and multiple ocean based human activities including fishing, marine transportation, and offshore wind energy development.

Index Terms:

4512 Currents, 4513 Decadal ocean variability, 4528 Fronts and jets, 4532 General circulation, 4594 Instruments and techniques

Keywords

Remote sensing; High Frequency Radar

Introduction

The coastal ocean is an intricate system that forms the boundary between the land and the deep ocean. For shallow and wide continental shelves, such as those on the U.S. East Coast, dynamical factors such as topography, large scale circulation, wind, fresh water input, and turbulent dissipation play key roles in governing shelf circulation and dynamics. While the deep ocean experiences independent air-ocean and ocean-benthos interactions, the benthos of the shallow ocean affects the surface layer and in turn the associated along and cross shelf transport (Soulsby 1993). Wind and buoyancy forcing are critical to the flow and can quickly change the dynamics on time scales ranging from hours and days to seasons and years.

The Middle Atlantic Bight (MAB) supports a complex marine ecosystem and it has been a focus of coastal oceanographic research since the early 1900s (Bigelow and Sears 1935).

115 The continental shelf of the MAB extends from Cape Hatteras, NC in the south to Georges
116 Bank off Cape Cod, MA in the north. The prominent topographic features in this region
117 are the Hudson Shelf Valley (Lentz et al. 2014), Nantucket Shoals (Beardsley et al. 1985,
118 Limebruner and Beardsley 1982), and Great South Channel (Chen et al. 1995). The width
119 of the shelf gradually decreases from ~ 120 km south of Cape Cod down to ~40 km east of
120 Cape Hatteras. The isobaths are roughly parallel to the coastline except near the Hudson
121 Shelf Valley and the many shelfbreak canyons distributed throughout the MAB.

122 Beardsley and Boicourt (1981) present a review of the estuarine and coastal circulation of
123 the MAB. The first dynamical model for the MAB showed a southwest drift of shelf and
124 slope waters from Cape Cod toward Cape Hatteras (Sverdrup et al., 1942). Miller (1952)
125 later showed that there was strong variability about this mean drift in the form of eddies
126 and current filaments. Using arrays of long-term moorings, Lentz (2008) showed that the
127 depth averaged flow is aligned along the isobaths with the exception of the Hudson Shelf
128 Valley where the mean flow is shoreward up the shelf valley. Chapman and Beardsley
129 (1989) suggest that the origin of the shelf water is from glacial melt along the southern
130 Greenland coast that propagates south to the MAB as a buoyant coastal current. Beardsley
131 and Winant (1979) show that the southwest flow of this cold glacial water is primarily
132 driven as a boundary current connected to the larger scale circulation of the western North
133 Atlantic Ocean (Fleming, 2016, Pringle 2018, Levin 2018).

134 Technology allowed for more long-term measurements of currents, water temperature and
135 salinity, and meteorological forcing in the 1960's. Beardsley and Boicourt (1981) describe

much of the work using these longer time series confirming that transient currents modulate the mean southwest drift. The focus of dynamical research in the 1970's shifted from the mean southwest flow to the current variability. Beardsley et al. (1976) suggest that the current variability of the MAB is mostly wind-driven. Moores et al. (1976) show that the wind forcing driving this variability is predominately from the west/northwest except in the summer months when the wind is typically from the southwest. Ou et al. (1981) go on to show observationally that the variability is composed of a wind forced component and a larger scale free wave component that is not correlated with the wind and propagates downshelf. Using numerical simulations, Beardsley and Haidvogel (1981) confirm that these current fluctuations do have a local and non-local response. The local response is related to local geometry, topography and forcing while the non-local response is due to forcing "distant in time and space".

Beginning in the late 1990's and early 2000's, High Frequency Radar (HFR) surface current mapping technology was introduced to the region. These networks have supported circulation research in the region including near shore studies off the coast of New Jersey (Kohut et al. 2004), the response of the shelf water to tropical storms (Kohut et al. 2006), and the seasonal variability of the shelf circulation (Castelao et al. 2008, Dzwonkowski et al. 2009, Dzwonkowski et al. 2010, Gong et al. 2010). In the MAB, numerous studies have validated the HFR surface currents against more traditional in situ measurements (Haines et al. 2017, Kohut and Glenn, 2003; Kohut et al. 2006 IEEE; Kohut et al. 2012; Ullman and Codiga 2004) and, as a result, these data now support U.S. Coast Guard Search and

157 Rescue operations in the MAB and throughout the U.S. (Ullman et al. 2006; Roarty et al.
158 2010).

159 Since 2007, the Mid Atlantic Regional Association Coastal Ocean Observing System
160 (MARACOOS) has operated a regional HFR network consisting of approximately 41
161 radars. These systems have been maintained through a regional collaboration of eight
162 separate organizations (University of North Carolina (Chapel Hill), Center for Innovative
163 Technology, Old Dominion University, Rutgers University, University of Connecticut,
164 University of Rhode Island, University of Massachusetts (Dartmouth), and Woods Hole
165 Oceanographic Institution). The network provides hourly measurements of ocean surface
166 currents (i.e., representative of water depths of 0.3 – 2.5 m) within ~250 km of the coast,
167 over an area encompassing more than 190,000 km^2 of the ocean's surface, at resolutions of
168 1 km, 2 km, and 6 km. In this study, we focus on ten years of shelf-wide surface current
169 data provided by this network to examine the response of the surface current fields to local
170 wind forcing and river input over seasonal to annual time scales. The study utilizes wind
171 measurements from several coastal and at-sea wind sensors and river discharge data to
172 describe the response of the two-dimensional structure of the ocean surface flow to these
173 drivers and place that response in the context of atmospheric and oceanic flow features.
174 The paper is divided into the following sections. In section 3, we describe the methods
175 used to collect and process the MARACOOS surface current data set, the National Oceanic
176 and Atmospheric Administration (NOAA) weather buoy and Coastal-Marine Automated
177 Network (C-MAN) station wind data, and the United States Geological Service (USGS)

river discharge data. In section 4, we characterize the mean and variability of the surface flow, the mean wind over the area and the seasonality of the surface currents. In section 5, we will discuss the results and draw conclusions in section 6.

Methods and Data

Surface currents

Surface current measurements were collected in the MAB from 2007 to 2016 using data from sixteen 5 MHz SeaSondes manufactured by CODAR Ocean Sensors (Figure 1). The SeaSonde is a High Frequency radar that uses the Doppler shift of radio signals reflected off ocean surface wind waves to measure the component of the ocean current along a radial line towards or away from the station. The average depth of the measurement varies with radar frequency and is proportional to □/8□ where □ is the radar wavelength (60 m at a 5 MHz transmit frequency). This equates to an average depth measurement of 2.7 m (Paduan and Graber 1997, Stewart and Joy 1974). The 60 m radio waves are resonant with ocean waves having a wavelength of 30 m, which equate to waves with a period of 4.3 seconds in deep water. Each HFR station generated three hour averaged radial component velocity maps every hour; the data collection period for each hourly file was the file timestamp ±90 minutes. Each radar utilized a 1 Hz sweep rate for the radio signal and a 1024-point fast Fourier transform (FFT) for the Doppler processing. This resulted in a radial velocity resolution of approximately ±1.5 cm/s for each hourly radial vector map.

197 The hourly radial files were combined into hourly total surface currents using the optimal
198 interpolation scheme (Kim et al. 2008, Kohut et al. 2012). Total surface currents had a
199 spatial resolution of 6 km on the national HFR grid (Terrill et al. 2006). For each year of
200 surface current data from December 2006 through November 2016, the t_tide toolbox in
201 MATLAB (Pawlowicz et al 2002) was used to detide data in annual segments (December
202 1 – November 30, Gong et al. 2010). A 30-hour low-pass filter was then applied to the
203 detided data in order to remove any remaining high frequency variability. Only grid points
204 with at least 50% coverage (Gong et al. 2010) at a normalized uncertainty level under 0.6
205 (Kohut et al. 2012) in both the u-component and v-component over the year were included
206 in this analysis. All means, variance, and root mean square (RMS) described below are
207 calculated using the detided and low-pass filtered data that met these quality criteria.

208 Single-year seasonal means (winter: December 1 – February 29; spring: March 1 – May
209 31; summer: June 1 – August 31; autumn: September 1 – November 30) were created by
210 averaging the hourly data over the three-month period wherever the temporal coverage was
211 at least 50%; annual means were calculated with all hourly data over the 12-month period
212 from December 1 – November 30, since it had already passed the 50% temporal coverage
213 criteria. Decadal means for each season and for the full year were calculated by taking the
214 mean of all ten previously calculated means, so each year was weighted equally. Each grid
215 point had to contain at least five individual yearly means (i.e. 50% coverage) to be included
216 in the decadal mean.

For each single-year seasonal and annual mean, a corresponding within-year variance was calculated for both eastward and northward velocities using the hourly surface current data. The decadal seasonal and total intra annual variance was calculated by taking the mean of the ten individual-year seasonal and total variances. The inter annual variance was calculated by taking the variance of the eastward and northward components of the ten individual-year seasonal and annual mean current fields. For each within- and between-year variance estimate, a corresponding root mean square error (RMS) value was calculated by taking the square root of the sum of the eastward and northward variance values; this RMS considers variation in both current speed and current direction. The same 50% coverage requirements applied to the mean currents were also used for variance and RMS.

The confidence interval of the surface currents on the continental shelf were computed for the decadal mean as well as the seasonal means on the continental shelf following Emery and Thomson (2014). The 95% confidence interval was calculated using the equation $1.96\sigma/(N^*)^{1/2}$ where σ is the standard deviation and N* is the effective degrees of freedom. N* was calculated using this equation $N^*=N\Delta t/T$ where N is the number of samples, Δt is the sampling interval (1 hour) and T is the integral time scale. T was calculated to be 19 hours from a year's worth of data at midshelf offshore of New Jersey, hence N* was 4,870 for the decade of data and was 1,218 for each of the seasons. The uncertainty amounted to ±0.2-0.6 cm/s for the decadal mean and within ±0.4-1.0 cm/s for the seasonal means.

Winds

Wind data from ten NOAA National Data Buoy Center (NDBC) stations (44008, 44009,44014, 44017, 44020, 44025, 44065, 44066, chlv2 and ocim2) were used for the wind analysis. Hourly wind data over the ten-year record from 2007 to 2016 were accessed from (https://www.ndbc.noaa.gov). A minimum of 50% temporal coverage was required of the annual or seasonal record to be included in the analysis. The wind data was averaged in the same manner as the current data to generate the seasonal means. The statistics of the wind speed and direction were performed by converting wind speed and direction into an east and north vector; all the east vectors were averaged and all the north vectors were averaged and then the resulting two vectors were combined to obtain a mean wind vector. This mean wind vector was then converted back into a magnitude and direction from.

River Discharge

Daily river discharge data were collected from the U.S. Geological Survey (USGS) water data available online (http://waterdata.usgs.gov/nwis) for the Connecticut and Delaware rivers. Discharge data from the Hudson, Mohawk, Passaic, and Raritan rivers were combined into a single product and labeled the Hudson River. Discharge data from the Susquehanna, Potomac, Patuxent, Rappahannock, Choptank, James, Appomatox, Pamunkey and Mattaponi rivers were combined into a single data set and labeled the Chesapeake. The USGS station number corresponding to each river is given in Table 1. The discharge data from the individual stations were merged following the methodology

of Chant (2008) and Zhang (2009). The final discharge data sets are made available on the Rutgers ERDDAP server (http://tds.marine.rutgers.edu/erddap/tabledap/ROMS_DISCHARGE.graph).

Results

Decadal Mean Surface Currents

Throughout the manuscript wind direction will follow the meteorological convention where direction indicates where the wind is blowing from and the currents will be described in the oceanographic convention where direction indicates where the current is flowing towards. The wind field as observed by the ten wind sensors in the region show a mean wind from the west northwest that increases speed with distance offshore and rotates slightly to be out of the northwest near the shelf break (Figure 2a). Wind variability is denoted by 95% confidence ellipses with a scale of 15 m/s. The mean surface flow over the ten-year period (2007-2016) as measured by the MARACOOS long-range HF radar network was offshore and equatorward with a speed of 2-12 cm/s (Figure 2b) with the mean across the entire field of 7 cm/s. The alongshelf currents increase with increasing water depth, consistent with Lentz (2008). Compared to the mean, the currents are most steady along the shelfbreak and most varied near the coastline, essentially varying in offshore direction in concert with the change in coastline orientation. North of the Hudson Shelf Valley (HSV) the currents are toward the southwest while south of the HSV the

currents are towards the southeast rotating clockwise toward the southwest with distance offshore. This agrees with the earlier work by Gong et al. (2010) who observed the HSV divides the flow into two regimes north and south of the valley. The currents gradually transition from SE to SW with increasing depth; southward currents are centered along the 50 m isobath from Virginia to New Jersey. The surface currents strengthen seaward of the 50 m isobath with speed increasing to 7–11 cm/s with faster flow observed further south. South of the Chesapeake Bay (CB), the flow then turns offshore and merges with the Gulf Stream. The broad band of fast flowing current over the outershelf and shelfbreak is persistent throughout most of the year and it is thought to be associated with the meandering shelfbreak jet (Linder and Gawarkiewicz 2004). However, other factors such as buoyancy driven flow from the rivers also likely contributed to this enhanced flow feature. For our purpose, we will continue to call it the shelfbreak jet, but please keep in mind that this is only in a statistical sense. Any synoptic realization of the shelfbreak jet will likely look very different then this average view.

The surface flow east of Cape Cod is predominantly to the southeast. Below Cape Cod, the flow turns toward the southwest to join the flow south of Rhode Island. Moving south from Cape Cod the mean surface flow is along isobath towards the equator, consistent with previous studies that analyzed the depth-averaged flow with current meters (Beardsley and Boicourt 1981, Lentz 2008) and HF radar (Gong 2010).

The weakest flow regions are observed near the New York Bight apex and south of Cape Cod where the surface currents drop to between 1 and 3 cm/s. The strongest flows in the

region are observed near the Gulf Stream, east of Cape Cod and Nantucket and a strong coastal current along the coast of North Carolina (Lentz et al. 2003).

The influence of the rivers can be seen as the increased velocity regions near the eastern end of Long Island, south of the Hudson Shelf Valley, south of the Delaware Bay and the strengthened coastal current along the coast of North Carolina off of the Chesapeake.

Variability of Surface Currents

The variability of the surface current is significant compared to the mean. The standard deviation within a year (Figure 2d) is between 10-20 cm/s for the entire field reaching a peak of 20 cm/s off Cape Hatteras where the variability in the position of the Gulf Stream factors significantly (Andres, 2016). Marks representing one standard deviation in the east/west and north/south direction for every 5^{th} grid point are shown with a reference of 25 cm/s in the lower right of the figure. The average standard deviation for the entire field is 15 cm/s. The standard deviation in the northern portion of the domain is of the order 10 cm/s and gradually increases to 20 cm/s in the southern portion of the domain. While the climatological mean is towards the equator, the daily mean can be poleward or opposite the mean flow for several days if the wind conditions are from the south or southwest (Frey, 1978, Bumpus 1969). Two regions of lower variability are seen over the New Jersey shelf and off the Virginia/ North Carolina coast.

The variability from year to year is much less than the variability within the year. The average variability between years is 4 cm/s for the entirety of the domain (Figure 2c).

316 Marks representing one standard deviation in the zonal and meridional direction for every
317 5th grid point are shown with a reference of 10 cm/s in the lower right of the figure. The
318 variability between years increases across the shelf most likely due to the position of the
319 shelf break jet (Linder and Gawarkiewicz, 1998; Fratantoni and Pickart, 2003). The
320 variability between years is highest in the southern region extending up to 37.5 N latitude
321 where the location of the Gulf Stream may influence this variability.

322 ## Seasonal Mean Flow

323 The surface current and wind data were seasonally averaged following Flagg et al.'s (2006)
324 climatological analysis of the subsurface currents on the outer shelf and Gong et al.'s
325 (2010) analysis of the surface currents on the shelf. The following is a discussion of the
326 seasonally averaged winds (Figure 3) and currents (Figure 4). Again, the variability in the
327 winds are denoted by 95% confidence ellipses. Note that the maps of the seasonal winds
328 and currents are arranged with winter in the upper left and progressing clockwise through
329 the seasons to make it easier for the reader to identify the season to season changes in
330 adjacent maps.

331 To describe the regional differences in surface transport, the continental shelf off the
332 northeast US is divided into four distinct regions, by combining some of the same regional
333 definitions used by Wallace et al. (2018) in their hydrographic analysis. From north to
334 south, the four analysis regions are Region 1 encompassing Eastern New England (ENE),
335 Region 2 encompassing Southern New England (SNE) and New York Bight 1 (NYB1),
336 Region 3 encompassing New York Bight 2 (NYB2) and Southern Shelf 1 (SS1), and

Region 4 encompassing Southern Shelf 2 (SS2). In addition, we defined the Mid-Atlantic Bight (MAB) region as encompassing the three southern-most regions (similar to the regions defined by Mountain (2003) but modified to better encompass the inner shelf domains). These regions are illustrated in Figure 1. We focused the wind analysis on four stations as being representative of the wind field within the particular regions: Region 1 (44008), Region 2 (44025), Region 3 (44009) and Region 4 (44014).

The seasonal maps of the ten-year average HFR surface current and NOAA buoy winds reveal the following:

Winter, from December to February, strong winds from the west northwest are present over the entire area (Figure 3a), and the flow is similar to the long-term mean (Figure 4a). The ocean surface currents are predominantly offshore, only slightly to the right of the winds with peak velocities between 7 and 12 cm/s. The core of the shelfbreak jet has moved offshore to over the 1000 m isobath. The current response was divided into four sub regions which allows for a finer description of the flow. 1) ENE, flow to the east over Nantucket Shoals diverges to east and south. 2) SNE & NYB1 – currents are toward the south on inner shelf turning to the south southwest as they cross the shelf break. The low current area south of Nantucket has slightly increased speeds compared to the decadal mean and currents are directed much more to the south. 3) NYB2 & SS1 – currents are offshore toward the southeast over the inner shelf turning south as they cross the shelf break, and lastly region 4) SS2 - currents are alongshelf turning counter clockwise to transport water off of the shelf into the Gulf Stream.

Spring, from March to May, weak winds from the west are present nearshore (Figure 3b) with slightly stronger winds in the eastern portion of the domain. The currents inshore of the 100 m isobath are weaker than winter with velocities of 3-6 cm/s. Stronger alongshore currents persist offshore of the 100 m isobath in the range of 9-12 cm/s (Figure 4b). There is a distinct continuous shelfbreak jet, with a wide peak that starts south of Martha's Vineyard and runs continuously until it turns offshore before reaching Cape Hatteras. 1) ENE – again currents are to the southeast and south to the right of the wind are observed. 2) SNE & NYB1 – Currents are to south southwest over most of the shelf with south and south southeast currents near the Hudson Shelf Valley. South of Nantucket, there are weak currents to the southwest, opposite of the wind. 3) NYB2 & SS1 – currents to the southeast over inner shelf, turning to southwest over outer shelf. 4) SS2 - outflow hugs the coastline, turns with the coast, and is then transported offshore into the Gulf Stream. There is a pathway from the shelf/slope front to the east into the Gulf Stream as far north as Chesapeake Bay.

Summer, from June to August, the winds are at the midrange of speeds (1.0 to 1.9 m/s) and from the southwest (Figure 3d), typical of the large-scale response to the summer Bermuda high (Zhu and Liang, 2013). Summer has the weakest flows of all the seasons with currents of 3-6 cm/s over most of the shelf (Figure 4d). The currents along the 100 m isobath are slightly faster than those inshore of that isobath. Currents are predominantly offshore, about 90 degrees to the right of the winds in this highly stratified season with peak velocities, 6-8 cm/s, over the 100 m isobath. 1) ENE - There is an area of weak

currents and divergence southeast of Nantucket. North of this there are strong currents to the southeast. 2) SNE & NYB1 – Currents are south southwest over most of the shelf. South of Nantucket and Martha's Vineyard, there are weak west to southwest flows and a small area south of Nantucket has northwest to north northwest flow that is not present in any other season. Strong flows from Long Island and Block Island Sounds are offshore to the southwest. 3) NYB2 & SS1 – The cross-shore flow extends further out over the shelf before turning more alongshore and the inner-shelf flow is weaker than in other seasons. 4) SS2– weaker flow and directed more cross-shelf than in the other seasons, transporting water to the southeast off the shelf towards the Gulf Stream.

Fall, from September to November, has similar medium wind speeds as summer but are turned to be from the northwest, in the offshore direction (Figure 3c). Fall displays the fastest currents of all the seasons with currents greater than 6 cm/s over most of the shelf (Figure 4c). Compared to summer, the currents across most of the shelf increase in speed, especially off Maryland and Virginia where they accelerate to 13 cm/s along the 80m isobath. The shelfbreak jet is the strongest and widest in fall with peak currents beginning south of Martha's Vineyard. The broad peak extends between the 60 m and > 1000 m isobaths. This feature flows all the way south to join the Chesapeake outflow and flow offshore to the Gulf Stream in one wide region. 1) ENE – the flow is to east over Nantucket Shoals. Southeast of Nantucket, there are slower currents directed to the southeast. 2) SNE & NYB1- south-southwest currents on the inner shelf turn slightly to the southwest over the outer shelf, accelerating in the alongshelf direction. 3) NYB2 & SS1 – on the inner

shelf the currents are offshore and towards the south, turning to alongshelf over the mid to outer shelf. At the outer shelf and in the slope water the currents are alongshelf, 90 degrees to the right of wind. 4) SS2 - outflow along the coast is strong and joins the shelfbreak jet over the shelf and both flow offshore in one current

The seasonal mean and standard deviation of the discharge (m^3/s) for each of the 4 major rivers in the MAB are shown as tables in Figure 3. The outflow from the Connecticut, Delaware and Hudson are of the same order while the outflow from the Chesapeake is 2-4 times larger than each of these rivers. The largest outflow is in the spring accounting for 40% of the fresh water into the system with the lowest discharge in the summer only accounting for 15%. This pattern also holds true for the variability with the spring accounting for 21% of the variability (one standard deviation) and the summer accounting for only 6% of the variability.

Alongshelf and Cross Shelf Flows

In this section a quantitative description of the seasonal flow in the MAB is provided. The alongshore and cross-shore current was calculated over a mid-shelf line (Figure 5a) and the distance in kilometers along the line is overlaid on the line where the origin is east of Cape Hatteras and increases towards the north. The bearing along this line was used to rotate the surface currents into an along isobath and cross isobath coordinate system. The new current components were then plotted as a function of distance along the isobath as shown in Figure 6a for the alongshelf flow and Figure 6b for the cross-shore flow. The approximate location of where the four major estuaries connect to the shelf water are drawn

421 as horizontal lines in Figure 6, Chesapeake Bay at distance marker 150 km, Delaware Bay
422 at 350 km, Hudson River at 550 km and Long Island Sound at 700 km.

423 Three distinct regions emerge from these plots. The first region from 0 km to 150 km is
424 where the shelf slope front turns offshore and the Chesapeake Bay plume accelerates along
425 the coast and the two flows join with the Gulf Stream to be advected to the northeast.
426 Within this region there is an increase in both the alongshelf flow and cross-shelf flow.
427 The cross-shelf flows are consistent from season to season. Winter and fall display the
428 greatest alongshelf flow while summer exhibits the weakest alongshelf flow. Spring
429 resides in the middle with an alongshelf flow of 4 cm/s near Chesapeake Bay accelerating
430 to 9 cm/s near Cape Hatteras. The second region is from 800 to 900 km where the along
431 shelf flow is consistent between the four seasons. The cross-shelf flow is 1-4 cm/s while
432 winter exhibits the strongest cross shore flow due to the strong northwest winds.

433 Lastly, the third region between 150 to 800 km shows a consistent alongshelf flow and then
434 an increase during some seasons when you reach 350 km in the vicinity of Delaware Bay.
435 The alongshelf flow is strongest in the fall and weakest in the summer. The cross-shelf
436 flow is offshore for each season and the alongshelf flow is equatorward in each season.
437 The cross-shelf flow is consistent between the seasons. There are local maximum points
438 in the cross-shelf flow near the major estuaries at Long Island Sound, Hudson Shelf Valley
439 and Delaware Bay. The cross-shelf flow then accelerates when it reaches Chesapeake Bay
440 at 150 km. South of the 350 km distance marker there is an increase in the alongshelf flow
441 except in summer. It is in this middle zone where all the variation in space and seasonality

takes place. In winter when the water column is well mixed the flow will be more influenced by topography while in the summer it will be influenced by the stratification.

The findings for distances 0-800 km along the mid-shelf line show a stronger cross shelf flow than measured by Lentz (2008) who found the cross-shelf flow to be between 1 and 3 cm/s near the surface. Lentz (2008) also noted that the current meter records showed stronger offshore flows in the northern MAB and weaker cross shelf flows in the southern MAB. This agrees for the area off Cape Cod. We note an area of increased cross shelf flow off of Cape Hatteras.

Next, we looked at the behavior of the surface flow at the outershelf. Here we used a 4-minute bathymetry file isolating the 200 m isobath as a reference. Two bounding lines were constructed 50 km onshore and offshore of a smoothed 200 m isobath (Figure 5b). The surface currents were interpolated onto cross-isobath lines formed by connecting onshore and offshore points of the bounding lines. The currents were then rotated into an alongshore and cross-shore reference frame. The maximum alongshelf flow on each of these cross-isobath lines was identified and recorded. The location (Figure 7a) and magnitude (Figure 7b) of the maximum alongshelf flow by distance along the isobath is shown for each of the four seasons. The location of the contour line varies seasonally. South of the Hudson Shelf Valley, the outer-shelf maximum alongshore velocity is furthest offshore in the winter and furthest inshore in summer. Past 750 km (east of Long Island in Figure 5b), the maximum velocity line is furthest inshore in winter and furthest offshore in

462 fall. Figure 7b shows an increase in the alongshore flow from the northern part of the MAB
463 to the southern extent.

464 ## Seasonal Variability

465 Next, we examined for each season the variability of the surface flow within the years
466 (intra-annual variability) and the variability between the years (interannual variability).
467 Intra-annual variability (Figure 8) is found by calculating the standard deviation of the
468 hourly data each season, then averaging the results for all ten years so that each year is
469 equally weighted. This provides a measure of the short-term variability expected within a
470 season. Inter-annual variability (Figure 9) is calculated by taking the standard deviation of
471 the ten annual averages. This provides a measure of the year to year variability in the
472 seasonal averages.

473 For the intraseasonal statistics, summer is the least variable with a standard deviation of
474 11.9 cm/s averaged over the entire field. Winter and fall exhibit the highest variability at
475 15.4 cm/s. Spring is in between at 14.5 cm/s. Comparing Figure 8 to Figure 4, the
476 standard deviation of the short-term variability is greater than the mean flow speeds. The
477 variability decreases with higher latitude in each of the seasons. Winter, spring and fall all
478 display less variability over the Hudson Shelf Valley. As noted by Gong et al. (2010) the
479 spatial variability of the surface currents are affected by different forcing mechanisms at
480 different scales. Wind forcing and stratification operate at shelf wide scales while
481 topography can influence the flow on scales of tens of kilometers.

The inter-seasonal variability is one third the value of the intra-seasonal, implying that the seasonal averages are relatively stable from year to year. For the inter-seasonal statistics, again summer is the least variable with a standard deviation of 3.5 cm/s for the whole field. The most significant year to year variability in the domain occurs in the southern half of the MAB, either along the shelfbreak jet or along on the southern MAB shelf itself, where the strong currents turn towards the shelf break and the Gulf Stream. The variability between summers is high near the eastern side of Long Island Sound which match the findings of Ullman and Codiga (2004) who found a surface-intensified jet that is strongest in the summer and essentially absent in winter. The variability is high between springs at the shelf break near 40°N, 71°W, an area where Gulf Stream warm core rings are known to impact the shelf (Zhang and Gawarkiewicz, 2015). The variability between seasons is relatively constant at 3 cm/s along the New Jersey and New York coast. The fall is unique in having both high inter and intra seasonal variability. We will focus on the variability associated with this season in the Discussion section.

Discussion

General Overview: Variability of Surface Circulation in MAB

A 10-year time series of surface ocean currents mapped with a long range HFR network identified important patterns and pathways in the mean and variance of the surface flow over annual and seasonal time scales. These data show that the variability in the flow over these time scales is twice the magnitude of the mean, driven by similar variance in the local

502 winds. The largest variability in the surface currents was typically seen in the fall and
503 winter seasons when the MAB transitions from a highly stratified water column to a well-
504 mixed water column. During these seasons energetic wind events and buoyancy inputs
505 drive the observed variability.

506 The seasonally-averaged winds and the variabilities of the winds for the MAB are shown
507 in Figure 3. Autumn and winter generally exhibit stronger winds in the cross-shore
508 direction from the northwest, with more spatial variability in the autumn when the winds
509 are slightly weaker. Progressing from spring into summer, the weaker winds are more
510 alongshore from the southwest, with more spatial variability in the weaker spring.
511 Freshwater input can also be divided into two types of response, but offset in time from the
512 winds. Freshwater input is typically largest in winter and spring, and lowest in summer
513 and fall. In fall and winter, cross-shore winds are dominant with low riverine flow in the
514 fall and high flow in the winter. On the other hand, spring and summer seasons exhibit
515 predominately alongshore winds with high riverine flow in the spring and low flow in the
516 summer.

517 The seasonal mean currents from Figure 4 indicate that fall and winter currents are very
518 similar, with the weakest currents inshore in the northern half of the MAB, and the highest
519 flows near the shelf break and across the entire shelf in the southern MAB. In winter, the
520 spatially consistent strong northwesterly winds may act to diminish the westward
521 alongshore component of flow in the northern MAB. This is quite different than the
522 southern MAB where the relative angle of the wind and shelf geometry is more

perpendicular and the alongshore transport is enhanced winds in the fall is more variable in directions. During this transition season, the flow is directed more alongshore. Spring and summer currents are similar in that both have weaker currents nearshore along the entire MAB, increasing in magnitude with distance offshore, with the strongest currents near the shelfbreak. The cross-shelf pathways are prominent in both the high flow spring and the low flow summer. During the high flow spring, the currents reach speeds similar to the wind driven currents of fall and winter despite having very little average wind forcing.

In general, moving from north to south along the mid-shelf line with the main current, the alongshore current speeds increase, peaking in Region 4 SS2 (Figure 6a). The alongshore current rapidly increases as the strong current turns offshore and exits the shelf over a seasonally variable 150-200 km wide region. Alongshore currents in the spring and summer are similar with the wind opposing the flow. Fall and winter have the largest alongshore currents, when the wind is cross-shore and the water column is generally less stratified. The alongshore flow is strengthened in the southern MAB in the fall and winter where there is a rotation in the wind to align with alongshore towards the south. Alongshore currents in the winter are the lowest in the northern MAB where they opposed by the local wind. South of the Hudson Shelf Valley, at the shelfbreak, the maximum in the alongshelf flow is found farther offshore in winter (Figure 7a) when the cross-shelf winds are the strongest and in spring when the river discharge is greatest. At midshelf, cross-shore currents are nearly 3-6 cm/s over much of the MAB except in the southern

MAB where the flow turns offshore and heads off the shelf. Local peaks in the cross-shelf flow occur at Long Island Sound (LIS), Hudson Shelf Valley (HSV) and Delaware Bay (DB) (Figure 6b).

Intra seasonal variability is similarly large in fall (high winds speeds) through winter (medium wind speeds and medium river flow) and into spring (low winds and high river flow), with significantly lower variability in the summer. Spring variability is smaller in the northern half of the MAB when winds are very low and the rivers have not had their influence. In the southern MAB, the variability during the high flow season from the Chesapeake is similar to the variability during the fall and winter.

Inter annual variability shows that the year to year variation is greatest in the southern MAB offshore in the outflow region. Most of the year to year variability in the rest of the MAB is near the outer and inner edges of the shelf. Away from the outflow region, the fall has the largest variability, extending across the entire shelf. We therefore chose to look at the variability in the wind forcing and buoyancy inputs during the fall when we expect to see the most implications for shelf wide- differences.

Detailed Case Study: A Tale of Two Falls

The fall seasonal average wind velocity is plotted for the four main NDBC buoys in Figure 10a. The years 2009 and 2011 stand out as being different from the rest. For the fall 2009 season the winds are the strongest with little spatial variability over the entire MAB. The fall of 2009 was an anomalous wind year in that the winds were stronger and shifted

clockwise to be more northeasterly rather than the northwesterly winds typically observed in the fall. This was due in large part to the passage of 7 coastal low-pressure systems through the MAB including the extratropical system Nor'Ida (Olabarieta et al., 2012). The passage of each of these systems stalled in the bight apex which allowed for the counterclockwise flow around the cyclone to drive surface winds and, consequently surface currents, down the shelf (Figure 11a). The surface currents were aligned towards the southwest with weak cross shelf transport south of the bight apex.

The fall of 2011 was another anomalous fall for a different reason. This season had the weakest winds between the two buoys that reported. In 2011 there was a large amount of freshwater discharge due to the passage of Hurricane Irene (Glenn, et al 2016) and Tropical Storm Lee (Munroe, 2013). These weather systems delivered three times the typical seasonal rainfall (Figure 12) and hence discharge to the northern half of the region as evidenced by the discharge from the Connecticut, Delaware and Hudson Rivers. These storm systems made an even greater impact on the southern region of the domain by delivering five times the normal fall precipitation and discharge onto the shelf as measured by the discharge from the Chesapeake gauges (Figure 10b). The outflow from rivers are relatively steady but if an anomalous discharge like that of 2011 occurs, the ocean response is seen across the entire shelf. The response of the currents on the shelf to this increased discharge can be seen as a pronounced offshore surface transport near the exits of the four major estuaries with lower offshore transport between these pathways (Figure 11b).

584 In order to evaluate overarching meteorological conditions which may be influencing this
585 interannual variability we saw in 2009 and 2011, the synoptic weather types for each fall
586 during the 10-year period were examined using a synoptic typing dataset (Siegert et al.
587 (2016) and Suriano and Leathers (2017)). Synoptic typing aims to quantify common
588 features in the daily synoptic weather conditions in order to identify days that are similar.
589 The method utilizes an eigenvector approach described in Kalkstein and Corrigan (1986)
590 and Yarnal (1993) to classify synoptic conditions utilizing 4-times daily observations of
591 surface air temperature, dewpoint temperature, wind, sea level pressure, and cloud cover
592 dating back to 1948. The data was separated into the four meteorological seasons, and the
593 analysis of the principle components using the station observations was combined with a
594 visual qualitative analysis of NCEP/NCAR daily reanalysis (Kalnay et al., 1996) maps of
595 sea level pressure, 500 hPa geopotential height, surface air temperature, and surface
596 precipitation rates. The dataset has been used to evaluate hydroclimatology in the Mid-
597 Atlantic (Siegert et al., 2016), snowfall in the Great Lakes region (Suriano and Leathers,
598 2017), wind ramp events in the Mid-Atlantic Bight (Veron et al., 2018), and high ozone
599 pollution events in Delaware (Archer et al., 2018), showing broad applicability to weather-
600 related studies throughout the region.

601 We examined the daily distribution of synoptic types for the fall season
602 (September/October/November) of the dataset (2007-2016), thereby covering the 10 years
603 of the HF radar record. The synoptic typing dataset identified 14 different types during the
604 autumn season. From this analysis, the synoptic type classified as having a strong high-

605 pressure center over New England (spatial average in Figure 13b) emerged as the most
606 prevalent synoptic type during fall 2009, with 26 occurrences out of 92 days in the season,
607 more than any other year in the 10-year period. The New England High is centered overland
608 to the north, producing large scale winds also from the northeast over the MAB.
609 Additionally, several of the New England High cases also included coastal low pressure
610 over the South Atlantic Bight, further reinforcing this onshore wind flow pattern. This
611 indicates that the overall flow pattern over the Mid-Atlantic Bight was likely dominated by
612 both the New England High and earlier discussed coastal storms (Olabarieta et al., 2012),
613 helping to explain the strong average wind from the northeast seen in Figure 10a during
614 2009. However, 2011 (Figure 13a, blue bars) does not stand out as being an unusual year
615 for the New England High synoptic type, and so the river discharge and buoyancy forcing
616 would likely be more important forcing factors to help explain the surface current response
617 in the fall of 2011. The events responsible for the high river discharge anomaly
618 experienced in 2011 are compared to 2009 in Figure 12. River discharge for 2009 is low
619 and steady over the entire fall. In contrast, river discharge in 2011 shows the impact of
620 several storms, including two named tropical storms (Irene and Lee) and additional
621 northeasters. Tropical storms like Irene transited the MAB in less than 12 hours, but the
622 increase in river discharge from the tropical storm rains can last for days.

623 The fall seasonally averaged surface current maps are compared for 2009 and 2011 in
624 Figure 11. The fall 2009 currents (Figure 11a) are strong across the entire shelf, running
625 alongshelf in nearly the same direction as the wind until reaching the southern MAB where

626 the current turns more offshore. In the fall of 2011 (Figure 11b), currents are weak over the
627 inner shelf, and stronger over the outer shelf, with an offshore component nearly equal to
628 the downshelf component. Unlike 2009, offshore transport at the shelfbreak is observed
629 along the entire Mid Atlantic, not just in the far southern region. The strong cross-shelf
630 currents regions extend inward nearly to the coast near the four estuaries. In between the
631 four estuaries, the weak inner shelf currents extend to midshelf. The vastly different
632 surface regimes experienced in 2009 and 2011 point to the possibility that different
633 subsurface regimes are also present. Strong surface currents in the direction of the wind in
634 2009 are consistent with shallow water Ekman theory for an unstratified shelf. The large
635 buoyancy inputs from the estuaries in 2011 are expected to enhance stratification, which
636 acts to decouple the surface boundary layer from the bottom boundary layer (Chant et al.
637 2008).

638 ## Oceanographic and Ecological Implications

639 The implication of the different forcing on the shelf goes beyond those described in the
640 surface current fields above. As has been stated, the fall season marks a significant
641 transition in the MAB as it shifts from a strongly stratified two-layer system to a well-
642 mixed homogenized water column. Using autonomous underwater glider sections along
643 the Endurance Line from Tuckerton, NJ to the shelf break (Castelao et al. 2008) we
644 describe the oceanographic implications on the shelf hydrography (Figure 14). A glider
645 deployed in the fall of 2009 as part of an Observing System Simulation Experiment
646 (Schofield et al. 2010; Wang et al., 2013), indicates that the surface was cool (around 18

647 degrees C, Figure 14a) with relatively high salinity nearshore (Figure 14c). The water
648 column was well mixed nearshore and thermocline was at a depth of 40 m. Cross-shelf
649 temperature and salinity sections indicate that the windy 2009 fall transition to well mixed
650 conditions was nearly complete by mid-November. The core of the cold pool was offshore,
651 starting at the 50 m isobath and extending to the 80 m isobath. The strong winds and
652 resulting surface currents drove strong downwelling throughout the season, pushing the
653 warm surface water up against the coast and forcing the cold pool offshore, resulting in a
654 well-mixed water column on the inner shelf. Upwelling of the cold pool had occurred on
655 the inner side of the stratified zone, with the well mixed shallow area cutting off access to
656 the coast (Austin and Lentz, 2002). Over much of the continental shelf this year, the wind
657 influence extends to the bottom.

658 In contrast, during the fall of 2011, a glider deployed in support of the Mid-Atlantic
659 Regional Association Coastal Ocean Observing System (MARACOOS) (Brown, 2012),
660 indicates that the surface waters were warmer at 20 degrees C (Figure 14b) and the salinity
661 nearshore was much lower (Figure 14d). These lower salinities are the result of much more
662 freshwater discharged from multiple storms including Irene and Lee that moved through
663 the area. The stratification was much stronger in 2011 with the thermocline present over
664 the entire shelf with a depth of 20 m nearshore deepening to 40 m offshore. This intense
665 MAB temperature and salinity stratification persisted at least through late November. This
666 cross-shelf section indicates that the cold pool extended across the entire shelf, even
667 inshore of the 20 m isobath. The strong stratification results in what Chant et al (2008)

characterize as a more slippery interface between the surface and bottom layers, working to decouple the surface layer response from the influence of the bottom. In the fall of 2011, the wind influence is confined to the surface layer over this glider section, while the bottom layer response is dominated by cross and alongshelf pressure gradients.

The 2009 and 2011 fall seasons exemplify the significant variability in the forcing, ocean surface response and hydrography throughout the water column and across the shelf. Consequently, these physical characteristics have impacts on the marine life in this region. Some 321 species of fish call the MAB home (Able and Fahay, 1998). These species have evolved with seasonal dependent phenologies that anticipate and take advantage of this physical variability. For example, certain flounder species, such as the summer flounder, will time their spawn with the MAB fall transition. Adults two or more years old spawn as they migrate in September through November (Wilk et al, 1980). Their larvae are neutrally buoyant and adrift at the surface for thirty days. Therefore, the connection between summer flounder spawning grounds and nursery grounds is based upon the transport of larvae in the fall. Given the observed currents in our 10-year dataset, the transport of these larvae and their success to recruit into the fishery depends on the local forcing. In 2009, when the alongshore currents were strong and to the southwest, these larvae were rapidly advected south. In 2011, when significant freshwater outflow lead to a more cross shore transport pathway, the larvae likely moved offshore much faster than down the shelf.

Conclusion

Surface current patterns on the MAB's broad seasonally-stratified continental shelf are highly influenced by variability in the wind field and the riverine inflow of fresh water. This study used a decade of hourly surface current maps from an HFR network that spans the full MAB combined with wind observations from meteorological buoys and coastal stations as well as river discharges from the national stream gauge network. Ten year annual and seasonal means, along with their interannual and intra-annual variability, were calculated to study the spatial patterns of the mean surface currents, and their relation to the mean wind and riverine forcing.

Generally, the 10-year annual mean surface currents are (a) offshore and weaker, about 3-6 cm/s, near the coast, (b) increase in speed to about 8-10 cm/s and rotate to an alongshore direction on the outer shelf, and (c) similarly increase in speed and rotate to flow offshore towards the Gulf Stream in the southern MAB. The year to year interannual variability is low, with a standard deviation of about 1-3 cm/s over most of the shelf, but the variability within a year is much greater, with a typical standard deviation of 10-20 cm/sec over the same region.

Compared to the annual mean, the four 10-year seasonal mean surface current maps generally exhibit similar spatial patterns but with different current magnitudes and slightly different directions, with winter and summer more cross-shore and the transition seasons of fall and spring more alongshore. Fall and winter, with their strong cross-shore mean

winds, have the strongest mean currents, while summer, with its opposing alongshore mean winds, have the weakest mean currents. Again, compared to the seasonal means, the seasonal interannual variability is lower, and the seasonal intra-annual variability is higher.

The season with the most variability was the fall, when the MAB transitions from highly stratified summer conditions to well mixed winter conditions. Examination of the annual wind and river discharge records indicate that fall of 2009 experienced an anomalously strong and coherent wind field over the MAB, while fall of 2011 had anomalously high river discharges due to a series of tropical and extratropical rainstorms. The spatial patterns of surface currents for these two fall seasons are different, with the relatively windy dry fall of 2009 exhibiting strong (8-10 cm/s) alongshore currents to the southwest over the entire MAB, while the low wind but rainy fall of 2011 exhibited weak (1-4 cm/s) cross-shelf currents over much of the inner shelf with cross-shelf peaks near the rivers. Cross-shelf temperature and salinity sections indicate that the windy 2009 fall transition to well mixed conditions was nearly complete by mid-November, but that in the wet fall of 2011, the intense MAB temperature and salinity stratification persisted at least through late November.

The MAB is the southern half of the Northeast United States Large Marine Ecosystem (LME). Long-term surface current observations, especially over seasonal time scales, provide insights into the physical conditions organisms have adapted to in these productive waters. Larvae that are neutrally buoyant are advected by these currents. Temperature sensitive fish migrate across-shelf based on the timing of the seasonal transitions. The

MAB is also a densely populated urbanized coast that supports multiple human activities, including fishing, marine transportation, and a developing offshore wind energy industry. Improved understanding of the mean currents and their variability will enable more informed development, better management of pollutants, and response to events, both natural and human-made.

Acknowledgements

The authors would like to recognize the effort of the technical team that kept the radar stations operating during this ten-year period that included Rich Arena, Chris Jakubiak, Zhitao Yu and Colin Evans.

Datasets for this research are available in these in-text data citation reference: Roarty. (2020), [Creative Commons Attribution 4.0 International].

Roarty, Hugh. (2020). 2007-2016 Surface Circulation over the Mid Atlantic Bight Continental Shelf derived from a Decade of High Frequency Radar Observations (Version version 01) [Data set]. Zenodo. http://doi.org/10.5281/zenodo.3770921

The MARACOOS HFR network was supported from 2007-2010 by NOAA Award NA07NOS4730221 “Phased Deployment and Operation of the Mid-Atlantic Regional Coastal Ocean Observing System (MARCOOS)”and from 2011-2016 by NOAA Award Number NA11NOS0120038 “Towards a Comprehensive Mid-Atlantic Regional Association Coastal Ocean Observing System (MARACOOS)”. Sponsor: National Ocean

Service (NOS), National Oceanic and Atmospheric Administration (NOAA) NOAA-NOS-IOOS-2011-2002515 / CFDA: 11.012, Integrated Ocean Observing System Topic Area 1: Continued Development of Regional Coastal Ocean Observing Systems. The MARACOOS HFR network was supported from 2016-2021 by NOAA Award Number NOAA-NOS-IOOS-2016-2004378 “MARACOOS: Preparing for a Changing Mid-Atlantic”.

References

Able, K. W. and Fahay, M. P., The first year in the life of estuarine fishes in the Middle Atlantic Bight. Rutgers University Press New Brunswick, New Jersey, 1998.

Andres, M. (2016). "On the recent destabilization of the Gulf Stream path downstream of Cape Hatteras." Geophysical Research Letters **43**(18): 9836-9842.

Archer, C. L., Brodie, J. F., & Rauscher, S. A. (2019). Global warming will aggravate ozone pollution in the US Mid-Atlantic. Journal of Applied Meteorology and Climatology, 58(6), 1267-1278.

Austin, J. A. and S. J. Lentz (2002). "The Inner Shelf Response to Wind-Driven Upwelling and Downwelling." Journal of Physical Oceanography **32**(7): 2171-2193.

Beardsley, R. (1976). "Physical oceanography of the middle Atlantic Bight." Middle Atlantic Continental Shelf and the New York Bight.

Beardsley, R. C., W. Boicourt and D. Hansen (1976). CURRENT VARIABILITY AND MEAN CIRCULATION IN MIDDLE ATLANTIC BIGHT. TRANSACTIONS-AMERICAN GEOPHYSICAL UNION, AMER GEOPHYSICAL UNION 2000 FLORIDA AVE NW, WASHINGTON, DC 20009.

Beardsley, R. C. and D. B. Haidvogel (1981). "Model Studies of the Wind-Driven Transient Circulation in the Middle Atlantic Bight. Part 1: Adiabatic Boundary Conditions." Journal of Physical Oceanography **11**(3): 355-375.

Beardsley, R. C., D. C. Chapman, K. H. Brink, S. R. Ramp and R. Schlitz (1985). "The Nantucket Shoals Flux Experiment (NSFE79). Part I: A basic description of the current and temperature variability." Journal of Physical Oceanography **15**(6): 713-748.

Beardsley, R. C. and W. Boicourt (1981). "On estuarine and continental-shelf circulation in the Middle Atlantic Bight." Evolution of Physical Oceanography: Scientific Surveys in Honor of Henry Stommel **1**: 198-235.

790 Beardsley, R. and C. Winant (1979). "On the mean circulation in the Mid-Atlantic Bight."
791 Journal of Physical Oceanography **9**(3): 612-619.
792
793 Brodziak, J. and L. O'Brien (2005). "Do environmental factors affect recruits per spawner
794 anomalies of New England groundfish?" ICES Journal of Marine Science 62(7): 1394-
795 1407.
796
797 Brown, W., W. Boicourt, C. Flagg, A. Gangopadhyay, O. Schofield, S. Glenn and J. Kohut
798 (2012). Mapping the Mid-Atlantic Cold Pool evolution and variability with ocean gliders
799 and numerical models. 2012 Oceans.
800
801 Bumpus, D. F. (1969). "Reversals in Surface Drift in Middle Atlantic Bight Area." Deep-
802 Sea Research: 17-23.
803
804 Castelao, R., S. Glenn, O. Schofield, R. Chant, J. Wilkin and J. Kohut (2008). "Seasonal
805 evolution of hydrographic fields in the central Middle Atlantic Bight from glider
806 observations." Geophys. Res. Lett. **35**(3): L03617.
807
808 Chant, R. J., S. M. Glenn, E. Hunter, J. Kohut, R. F. Chen, R. W. Houghton, J. Bosch and
809 O. Schofield (2008). "Bulge Formation of a Buoyant River Outflow." J. Geophys. Res.
810 **113**(C1): C01017.

Chapman, D. C. and R. C. Beardsley (1989). "On the origin of shelf water in the Middle Atlantic Bight." Journal of Physical Oceanography **19**(3): 384-391.

Chen, C., R. C. Beardsley and R. Limeburner (1995). "Variability of currents in late spring in the northern Great South Channel." Continental Shelf Research **15**(4-5): 451-473.

Chen, X. and K.-K. Tung (2018). "Global surface warming enhanced by weak Atlantic overturning circulation." Nature **559**(7714): 387.

Drijfhout, S., G. J. Van Oldenborgh and A. Cimatoribus (2012). "Is a decline of AMOC causing the warming hole above the North Atlantic in observed and modeled warming patterns?" Journal of Climate **25**(24): 8373-8379.

Dzwonkowski, B., J. T. Kohut and X.-H. Yan (2009). "Seasonal differences in wind-driven across-shelf forcing and response relationships in the shelf surface layer of the central Mid-Atlantic Bight." J. Geophys. Res. **114**(C8): C08018.

Dzwonkowski, B., B. L. Lipphardt Jr, J. T. Kohut, X.-H. Yan and R. W. Garvine (2010). "Synoptic measurements of episodic offshore flow events in the central mid-Atlantic Bight." Continental Shelf Research **30**(12): 1373-1386.

Thomson, R. E., & Emery, W. J. (2014). Data analysis methods in physical oceanography: Newnes.

Flagg, C. N., M. Dunn, D. P. Wang, H. T. Rossby and R. L. Benway (2006). "A study of the currents of the outer shelf and upper slope from a decade of shipboard ADCP observations in the Middle Atlantic Bight." Journal of Geophysical Research: Oceans **111**(C6).

Fratantoni, P. and R. Pickart (2003). "Variability of the shelf break jet in the Middle Atlantic Bight: Internally or externally forced?" Journal of Geophysical Research: Oceans **108**(C5).

Frey, H. R. (1978). "Northeastward drift in the Northern Mid-Atlantic bight during late spring and summer 1976." Journal of Geophysical Research: Oceans **83**(C1): 503-504.

Gawarkiewicz, G., R. E. Todd, W. Zhang, J. Partida, A. Gangopadhyay, M.-U.-H. Monim, P. Fratantoni, A. M. Mercer and M. Dent (2018). "The changing nature of shelf-break exchange revealed by the OOI Pioneer Array." Oceanography **31**(1): 60-70.

852 Glenn, S., R. Arnone, T. Bergmann, W. P. Bissett, M. Crowley, J. Cullen, J. Gryzmski, D.
853 Haidvogel, J. Kohut and M. Moline (2004). "Biogeochemical impact of summertime
854 coastal upwelling on the New Jersey Shelf." Journal of Geophysical Research: Oceans
855 **109**(C12).
856
857 Glenn, S., T. Miles, G. Seroka, Y. Xu, R. Forney, F. Yu, H. Roarty, O. Schofield and J.
858 Kohut (2016). "Stratified coastal ocean interactions with tropical cyclones." Nature
859 communications **7**: 10887.
860
861 Goddard, P. B., J. Yin, S. M. Griffies and S. Zhang (2015). "An extreme event of sea-level
862 rise along the Northeast coast of North America in 2009–2010." Nature Communications
863 **6**: 6346.
864
865 Gong, D., J. T. Kohut and S. M. Glenn (2010). "Seasonal climatology of wind-driven
866 circulation on the New Jersey Shelf." J. Geophys. Res. **115**(C4): 25.
867
868 Haines, S., Seim, H., & Muglia, M. (2017). Implementing quality control of high-frequency
869 radar estimates and application to Gulf Stream surface currents. Journal of Atmospheric
870 and Oceanic Technology, 34(6), 1207-1224.
871

872 Hu, Z.-Z., A. Kumar, B. Huang, Y. Xue, W. Wang and B. Jha (2011). "Persistent
873 atmospheric and oceanic anomalies in the North Atlantic from summer 2009 to summer
874 2010." Journal of Climate 24(22): 5812-5830.
875
876 Kalkstein, L. S. and P. Corrigan (1986). "A synoptic climatological approach for
877 geographical analysis: assessment of sulfur dioxide concentrations." Annals of the
878 Association of American Geographers **76**(3): 381-395.
879
880 Kalnay, E., M. Kanamitsu, R. Kistler, W. Collins, D. Deaven, L. Gandin, M. Iredell, S.
881 Saha, G. White and J. Woollen (1996). "The NCEP/NCAR 40-year reanalysis project."
882 Bulletin of the American meteorological Society **77**(3): 437-472.
883
884 Kim, S. Y., E. J. Terrill and B. D. Cornuelle (2008). "Mapping surface currents from HF
885 radar radial velocity measurements using optimal interpolation." J. Geophys. Res.
886 **113**(C10): C10023.
887
888 Kohut, J. T. and S. M. Glenn (2003). "Improving HF Radar Surface Current Measurements
889 with Measured Antenna Beam Patterns." Journal of Atmospheric and Oceanic Technology
890 **20**(9): 1303-1316.
891

892 Kohut, J. T., S. M. Glenn and R. J. Chant (2004). "Seasonal current variability on the New
893 Jersey inner shelf." J. Geophys. Res. **109**(C7): C07S07.
894
895 Kohut, J. T., S. M. Glenn and J. D. Paduan (2006). "Inner shelf response to Tropical Storm
896 Floyd." J. Geophys. Res. **111**(C9): C09S91.
897
898 Kohut, J. T., H. J. Roarty and S. M. Glenn (2006). "Characterizing Observed
899 Environmental Variability with HF Doppler Radar Surface Current Mappers and Acoustic
900 Doppler Current Profilers: Environmental Variability in the Coastal Ocean." Oceanic
901 Engineering, IEEE Journal of **31**(4): 876-884.
902
903 Kohut, J., H. Roarty, E. Randall-Goodwin, S. Glenn and C. Lichtenwalner (2012).
904 "Evaluation of two algorithms for a network of coastal HF radars in the Mid-Atlantic
905 Bight." Ocean Dynamics **62**(6): 953-968.
906
907 Lentz, S. J., S. Elgar and R. Guza (2003). "Observations of the flow field near the nose of
908 a buoyant coastal current." Journal of physical oceanography **33**(4): 933-943.
909
910 Lentz, S. J. (2008). "Observations and a Model of the Mean Circulation over the Middle
911 Atlantic Bight Continental Shelf." Journal of Physical Oceanography **38**(6): 1203-1221
912

913 Limeburner, R. and R. C. Beardsley (1982). "The seasonal hydrography and circulation
914 over Nantucket Shoals." J. mar. Res **40**: 371-406.
915
916 Lentz, S. J., B. Butman and C. Harris (2014). "The vertical structure of the circulation and
917 dynamics in Hudson Shelf Valley." Journal of Geophysical Research: Oceans **119**(6):
918 3694-3713.
919
920 Limeburner, R. and R. C. Beardsley (1982). "The seasonal hydrography and circulation
921 over Nantucket Shoals." J. mar. Res **40**: 371-406.
922
923 Linder, C. A. and G. Gawarkiewicz (1998). "A climatology of the shelfbreak front in the
924 Middle Atlantic Bight." Journal of Geophysical Research: Oceans **103**(C9): 18405-18423.
925
926 Lipa, B., H. Parikh, D. Barrick, H. Roarty and S. Glenn (2013). "High-frequency radar
927 observations of the June 2013 US East Coast meteotsunami." Natural Hazards: 1-14.
928
929 Miller, A. R. (1952). A Pattern of Surface Coastal Circulation Inferred from Surface
930 Salinity-Temperature Data and Drift Bottle Recoveries, WOODS HOLE
931 OCEANOGRAPHIC INSTITUTION MASS.
932

933 Moores, C. N., J. Fernandez-Partagas and J. F. Price (1976). Meteorological forcing fields
934 of the New York Bight (first year's progress report), Tech. Rep. TR76–8, Rosenstiel School
935 of Mar. and Atmos. Sci., Univ. of Miami, Miami, Fla.
936
937 Mountain, D. G. (2003). Variability in the properties of Shelf Water in the Middle Atlantic
938 Bight, 1977–1999. Journal of Geophysical Research: Oceans, 108(C1).
939
940 Munroe, D., A. Tabatabai, I. Burt, D. Bushek, E. N. Powell and J. Wilkin (2013). "Oyster
941 mortality in Delaware Bay: Impacts and recovery from Hurricane Irene and Tropical Storm
942 Lee." Estuarine, Coastal and Shelf Science **135**: 209-219.
943
944 Olabarrieta, M., J. C. Warner, B. Armstrong, J. B. Zambon and R. He (2012). "Ocean–
945 atmosphere dynamics during Hurricane Ida and Nor'Ida: an application of the coupled
946 ocean–atmosphere–wave–sediment transport (COAWST) modeling system." Ocean
947 Modelling **43**: 112-137.
948
949 Ou, H. W., R. C. Beardsley, D. Mayer, W. C. Boicourt and B. Butman (1981). "An Analysis
950 of Subtidal Current Fluctuations in the Middle Atlantic Bight." Journal of Physical
951 Oceanography **11**(10): 1383-1392.
952

Paduan, J. D. and H. C. Graber (1997). "Introduction to high-frequency radar: Reality and myth." Oceanography **10**(2): 36-39.

Pawlowicz, R., B. Beardsley and S. Lentz (2002). "Classical tidal harmonic analysis including error estimates in MATLAB using T_TIDE." Computers & Geosciences **28**(8): 929-937.

Pettigrew, N. R., J. H. Churchill, C. D. Janzen, L. J. Mangum, R. P. Signell, A. C. Thomas, D. W. Townsend, J. P. Wallinga and H. Xue (2005). "The kinematic and hydrographic structure of the Gulf of Maine Coastal Current." Deep Sea Research Part II: Topical Studies in Oceanography 52(19): 2369-2391.

Roarty, H. J., S. M. Glenn, J. T. Kohut, D. Gong, E. Handel, E. Rivera Lemus, T. Garner, L. Atkinson, C. Jakubiak, W. Brown, M. Muglia, S. Haines and H. Seim (2010). "Operation and Application of a Regional High Frequency Radar Network in the Mid Atlantic Bight." Marine Technology Society Journal **44**(6): 133-145.

Roarty, Hugh. (2020). 2007-2016 Surface Circulation over the Mid Atlantic Bight Continental Shelf derived from a Decade of High Frequency Radar Observations (Version version 01) [Data set]. Zenodo. http://doi.org/10.5281/zenodo.3770921

974 Robinson, A. and S. Glenn (1999). "Adaptive sampling for ocean forecasting." Naval
975 Research Reviews **51**(2): 26-38.
976
977 Schofield, O., R. J. Chant, B. Cahill, R. Castelao, D. Gong, A. Kahl, J. Kohut, M. Montes-
978 Hugo, R. Ramadurai, P. Ramey, X. Yi and S. Glenn (2008). "The decadal view of the Mid-
979 Atlantic Bight from the COOLroom: Is our coastal system changing?" Oceanography
980 **21**(4): 108-117. https://doi.org/10.5670/oceanog.2008.08
981
982 Schofield, O., S. Glenn, J. Orcutt, M. Arrott, M. Meisinger, A. Gangopadhyay, W. Brown,
983 R. Signell, M. Moline and Y. Chao "others. 2010. Automated sensor networks to advance
984 ocean science." Eos Transactions, American Geophysical Union **91**(39): 345-346.
985 Siegert, C., D. Leathers and D. Levia (2017). "Synoptic typing: interdisciplinary
986 application methods with three practical hydroclimatological examples." Theoretical and
987 applied climatology **128**(3-4): 603-621.
988 Smeed, D., G. McCarthy, S. Cunningham, E. Frajka-Williams, D. Rayner, W. Johns, C.
989 Meinen, M. Baringer, B. Moat and A. Duchez (2014). "Observed decline of the Atlantic
990 meridional overturning circulation 2004–2012." Ocean Science **10**(1): 29-38
991 Soulsby, R. L., L. Hamm, G. Klopman, D. Myrhaug, R. R. Simons and G. P. Thomas
992 (1993). "Wave-current interaction within and outside the bottom boundary layer." Coastal
993 Engineering **21**(1): 41-69.

994 Stewart, R. H. and J. W. Joy (1974). HF radio measurements of surface currents. Deep sea
995 research and oceanographic abstracts, Elsevier.
996
997 Suriano, Z. J. and D. J. Leathers (2017). "Synoptic climatology of lake-effect snowfall
998 conditions in the eastern Great Lakes region." International Journal of Climatology **37**(12):
999 4377-4389.
1000
1001 Sverdrup, H. U., M. W. Johnson and R. H. Fleming (1942). The Oceans: Their physics,
1002 chemistry, and general biology, Prentice-Hall New York.
1003
1004 Terrill, E., M. Otero, L. Hazard, D. Conlee, J. Harlan, J. Kohut, P. Reuter, T. Cook, T.
1005 Harris and K. Lindquist (2006). Data Management and Real-time Distribution in the HF-
1006 Radar National Network. OCEANS 2006.
1007
1008 Ullman, D. S. and D. L. Codiga (2004). "Seasonal variation of a coastal jet in the Long
1009 Island Sound outflow region based on HF radar and Doppler current observations." J.
1010 Geophys. Res. 109(C7): C07S06.
1011
1012 Ullman, D. S., J. O'Donnell, J. Kohut, T. Fake and A. Allen (2006). "Trajectory prediction
1013 using HF radar surface currents: Monte Carlo simulations of prediction uncertainties." J.
1014 Geophys. Res. **111**(C12): C12005.

1015 Veron, D. E., J. F. Brodie, Y. A. Shirazi and J. R. Gilchrist (2018). "Modeling the electrical
1016 grid impact of wind ramp-up forecasting error offshore in the Mid-Atlantic region." Journal
1017 of Renewable and Sustainable Energy **10**(1): 013308.

1018 Wang, X., Y. Chao, D. R. Thompson, S. A. Chien, J. Farrara, P. Li, Q. Vu, H. Zhang, J. C.
1019 Levin and A. Gangopadhyay (2013). "Multi-model ensemble forecasting and glider path
1020 planning in the Mid-Atlantic Bight." Continental Shelf Research **63**: S223-S234.

1021 Wallace, E. J., Looney, L. B., & Gong, D. (2018). Multi-Decadal Trends and Variability
1022 in Temperature and Salinity in the Mid-Atlantic Bight, Georges Bank, and Gulf of Maine.
1023 Journal of Marine Research, 76(5), 163-215.

1024 Wilk, S.J., W. G. Smith, D.E. Ralph and J. Sibunka. (1980). The population structure of
1025 summer flounder between New York and Florida based on linear discriminant analysis.
1026 Trans. Am.Fish. Soc. 109:265-271.

1027 Yarnal, B. (1993). Synoptic climatology in environmental analysis: A primer. London,
1028 Belhaven Press.

1029 Zhang, W. G., J. L. Wilkin and R. J. Chant (2009). "Modeling the Pathways and Mean
1030 Dynamics of River Plume Dispersal in the New York Bight." Journal of Physical
1031 Oceanography **39**(5): 1167-1183.

1032 Zhang, W. G. and G. G. Gawarkiewicz (2015). "Dynamics of the direct intrusion of Gulf
1033 Stream ring water onto the Mid-Atlantic Bight shelf." Geophysical Research Letters
1034 42(18): 7687-7695.

1035 Zhu, J. and X.-Z. Liang (2013). "Impacts of the Bermuda High on Regional Climate and
1036 Ozone over the United States." Journal of Climate **26**(3): 1018-1032.

1037

Figure 1: Map of the Mid Atlantic Bight from Cape Hatteras, NC up to Cape Cod, MA. The locations of the 5 MHz HF radar stations are denoted as red triangles. NOAA NDBC stations are marked as black squares and labeled. The 50, 80, 200 and 1000 m isobaths are marked along with the 50% total vector coverage for the study period shown as the thick black line. The Tuckerton Endurance Line is marked in green. The continental shelf was divided into six regions following definitions used by Wallace et al. (2018). From north to south, the regions are Eastern New England (ENE), Southern New England (SNE), New York Bight 1 (NYB1), New York Bight 2 (NYB2), Southern Shelf 1 (SS1), and Southern Shelf 2 (SS2).

Figure 2: (a)Mean and 95% confidence ellipse of wind (m/s) from NDBC stations for 2007-2016. The reference vector of 2 m/s and 15 m/s variability ellipse is given in the lower right. Annual mean and standard deviation river discharge (m^3/s) from the four major estuaries within the MAB. (b) Mean surface current for the Mid Atlantic Bight (cm/s) colorbar indicates magnitude and vectors indicate direction towards of surface current (c)Interannual standard deviation of the surface currents (cm/s). (d) Intra-annual standard deviation of the surface currents (cm/s).

Figure 3: Map of mean and 95% confidence ellipse winds by season (a) winter, December-February (b) spring, March-May (c) fall, September-November and (d) summer, June-August. The reference vector of 2 m/s and 15 m/s variability ellipse is given in the lower right of each figure. The table insets provide the corresponding seasonal mean and standard deviation river discharge (m^3/s) from the four major estuaries within the MAB.

Figure 4: Mean surface currents (2007-2016) by season (a) winter, December -February (b) spring, March-May (c) fall, September-November and (d) summer, June-August. Colorbar indicates magnitude (cm/s) and vectors indicate direction towards of surface current.

Figure 5: (a) Reference line along the midshelf (red) used to calculate the cross shelf and alongshelf flow along the Mid Atlantic Bight and (b reference line along the 200 m isobath (red) and boundary lines (green) drawn 50 kilometers inshore and offshore of the isobath reference that were used to calculate the maximum alongshelf current. The numbers represent distance in kilometers along the reference line from south to north.

Figure 6: (a)Alongshelf current plotted by distance along the midshelf line (Figure 5a) by season winter (blue), spring(green), summer (black) and fall (red). (b) Cross-shelf current plotted by distance along the midshelf line. The

locations of the four major estuaries are denoted by the dotted lines Long Island Sound (LIS), Hudson Shelf Valley (HSV), Delaware Bay (DB) and Chesapeake Bay (CB).

Figure 7: (a) Location of maximum alongshelf current by season winter (blue), spring(green), summer (black) and fall (red). (b) Magnitude of the maximum alongshelf current plotted by distance along the Mid Atlantic by season.

Figure 8: Intra-annual standard deviation of the surface current in the Mid Atlantic from (a) winter, December-February (b) spring, March-May (c) fall, September-November (d) summer, June-August. One standard deviation marks in the east/west and north/south directions are shown for every 5th grid point (30 km spacing) with a reference scale of 25 cm/s in the lower right.

Figure 9: Interannual standard deviation of the surface current (cm/s) in the Mid Atlantic from (a) winter, December-February (b) spring, March-May (c) fall, September-November (d) summer, June-August. One standard deviation marks in the east/west and north/south directions are shown for every 5th grid point (30 km spacing) with a reference scale of 10 cm/s in the lower right.

Figure 10: (a) Mean winds from the four NDBC buoys in the fall season by year. (b) River discharge from four major rivers/estuaries for the fall season by year: Connecticut (red), Delaware (green), Hudson (blue) and Chesapeake (black).

Figure 11: Mean surface currents during the fall, September to November, of (a) 2009 and (b) 2011. Colorbar indicates magnitude (cm/s) and vectors indicate direction towards of surface current.

Figure 12: Time series plot of river discharge from four major rivers/estuaries for the fall of 2009 (top) and 2011 (bottom): Connecticut (red), Delaware (green), Hudson (blue) and Chesapeake (black).

Figure 13: New England High synoptic type classification for the period 2007-2016 where (a) shows the annual distribution of the synoptic type identified in the fall months (September/October/November). The 2009 year is highlighted in red, and the 2011 year is highlighted in blue. (b) The average map of sea level pressure from NCEP/NCAR reanalysis based on all days in the full synoptic dataset (1946-2015) for New England high pressure center (type 4010)

Figure 14: Temperature (top) and salinity (bottom) sections along the Tuckerton Endurance Line offshore of New Jersey for the fall of 2009 (left) and fall of 2011 (right).

1087

Table 1: List of river discharges that were utilized in the study. The Hudson and Chesapeake were an amalgamation of several rivers.

Major River	*Minor River*	*Location*	*USGS Station No.*
Connecticut		Thompsonville, CT	01184000
Hudson	Hudson	Fort Edwards, NY	01327750
	Mohawk	Cohoes, NY	01357500
	Passaic	Little Falls, NJ	01389500
	Raritan	Bound Brook, NJ	01403060
Delaware		Trenton, NJ	01463500
Chesapeake	Susquehanna	Conowingo, MD	01578310
	Potomac	Washington, DC	01646500
	Patuxet	Laurel, MD	01592500
	Rapphannock	Fredericksburg, VA	01668000
	Choptank	Greensboro, MD	01491000
	James	Cartersville, VA	02035000
	Appomattox	Matoaca, VA	02041650
	Pamunkey	Hanover, VA	01673000
	Mattaponi	Beulahville, VA	01674500